PARTICLE–LUNG INTERACTIONS

Edited by

Peter Gehr
University of Bern
Bern, Switzerland

Joachim Heyder
GSF–Research Center for Environment and Health
Neuherberg/Munich, Germany

MARCEL DEKKER

MARCEL DEKKER, INC.

NEW YORK · BASEL

5

Particle Deposition in the Respiratory Tract

HOLGER SCHULZ, PETER BRAND, and JOACHIM HEYDER

Institute for Inhalation Biology
GSF–Research Center for Environment and Health
Neuherberg/Munich, Germany

I. Introduction and Overview

During inhalation, particles are transported with the inspired air through the extrathoracic airways and the bifurcating tracheobronchiolar system to the gas-exchanging region of the lung. A certain number of these particles are caught in the respiratory system by touching the wet airspace surfaces, a phenomenon generally referred to as *particle deposition*. Therefore, with exhalation, not all particles are recovered. Figure 1A shows the fraction of particles deposited in the respiratory system (total deposition) during quiet mouth breathing as a function of the particle diameter. This fraction is small for particles in the size range between 0.1 and 1 μm. But it becomes larger for smaller and larger particles reaching almost 100% for 0.01- or 10-μm particles. However, the particle size determines not only how many particles are deposited, but also in which region of the respiratory tract these particles are deposited (regional deposition, see Fig. 1B–D). Total and regional deposition are modified further by other physical properties of the inhaled particles (particle density and shape), by the breathing pattern (tidal volume, breathing frequency, and flow rate; Fig. 2), and by the lung geometry (airspace dimensions).

The main question addressed in this chapter is: What is the impact of each

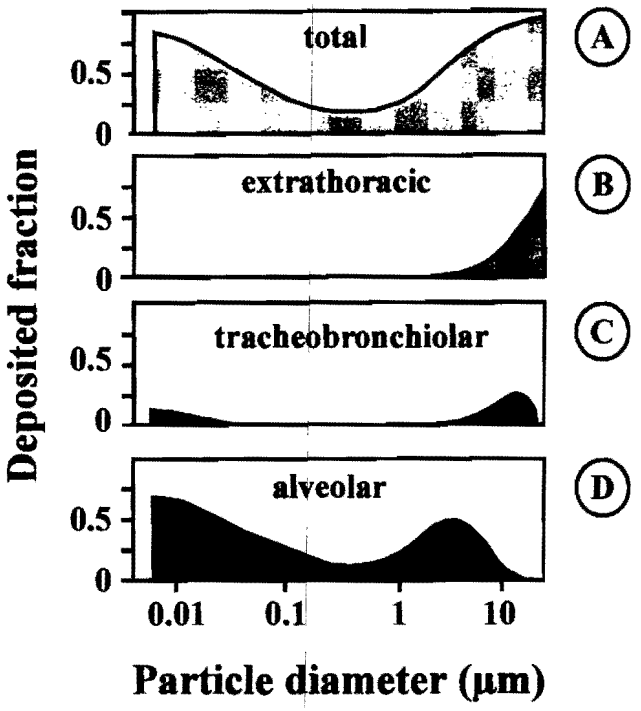

Figure 1 Schematic overview of (A) total deposition fraction and of deposition fraction in (B) the extrathoracic, (C) the tracheobronchial and (D) the alveolar region of the human respiratory system for unit-density spheres during mouth breathing. (From Ref. 163.)

of those factors on particle deposition and deposition pattern and, by knowing the significance of each factor, is it possible to target specific sites within the lung with particles inhaled for therapeutic or diagnostic purposes?

Particle Transport. Particle transport between mouth or nose and the alveoli is governed by convection, resulting from pressure gradients generated along the airways during breathing. Whereas convective bulk flow characterizes the displacement of particles toward the lung periphery or vice versa, convective mixing refers to the amalgam of inhaled with residual air. It occurs as a result of differences in bulk flow pattern during inspiration and expiration and nonuniform intrapulmonary ventilation (1–4).

As the total cross-sectional area of the airways increases rapidly toward the lung periphery (5), flow velocities and, hence, the linear velocity of bulk flow, decrease rapidly within airways from the extrathoracic to the small conducting airways and the alveolated region of the lung (4). Consequently, the residence time of particles is short within the large conducting airways, but increases toward the lung periphery.

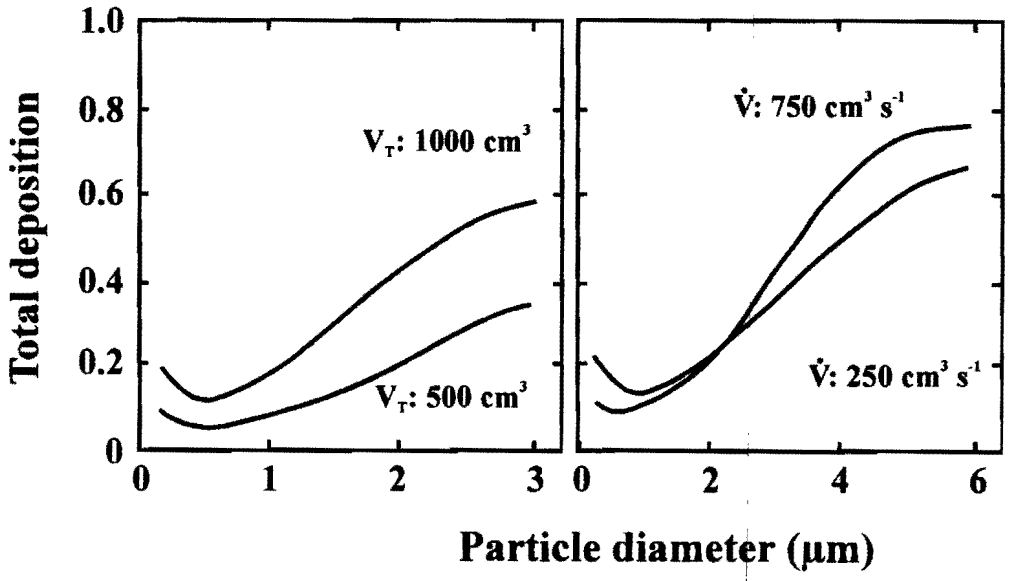

Figure 2 Effect of tidal volume (V_T: 500 cm^3 and 1000 cm^3) for a given flow rate of 250 cm^3 s^{-1} (left panel) and of flow rate ($\dot{V}$: 250 cm^3 s^{-1} and 750 cm^3 s^{-1}) for a given tidal volume of 1500 cm^3 (right panel) on total deposition fraction of unit density spheres. (From Ref. 10.)

Mechanisms of Mechanical Particle Transport. When particles do not follow, but diverge from, airflow streamlines and thereby come in contact with airspace surfaces, particle deposition occurs. This diverging from airflow streamlines and particle trajectories is mainly due to mechanisms of mechanical particle transport: inertial, gravitational, and diffusional particle transport (Fig. 3). The

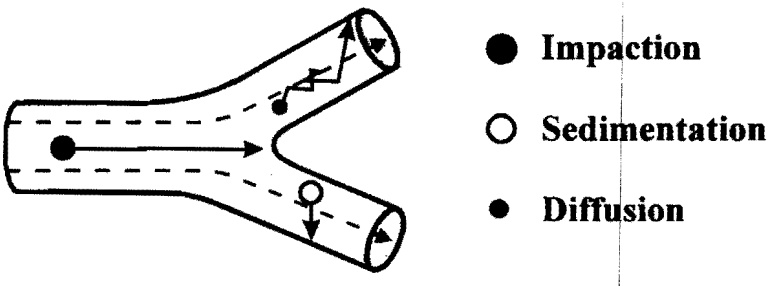

Figure 3 Mechanisms of particle deposition in the respiratory system. Illustrated are the three main deposition mechanisms, impaction, sedimentation, and diffusion, in an airway bifurcation during inhalation.

extent to which each of these mechanisms contributes to the deposition of a specific particle depends on the physical features of that particle.

Diffusion. For particles with a diameter less than 0.5 μm, particle displacement is governed mainly by diffusional transport. Collisions between gas molecules and a particle cause numerous very small random displacements of that particle. The distance a particle will travel by diffusion increases with time and with decreasing particle diameter (Table 1). A 0.1-μm particle can cover a distance of 40 μm in 1 s; a 0.01-μm particle a distance of 350 μm. Hence, the probability of particles to hit airspace surfaces by diffusional transport is larger the smaller the particles are and the longer they remain in the respiratory system. Consequently, the lung periphery with its small airway dimensions favors deposition by diffusion. Residence time is long, and the distance a particle has to travel before it hits an airspace wall is short.

Sedimentation. Particles are continually exposed to gravity and undergo gravitational settling (see Fig. 3). In contrast with diffusional transport, particle displacement by gravitational settling becomes significant for particles larger than 0.5 μm (see Table 1). The distance a particle settles within a given time increases with its mass (i.e., with its density and with its diameter). For instance, a unit-density sphere of 1-μm diameter settles at a distance of 35 μm in 1 s, whereas a unit-density sphere of 10-μm diameter settles at a distance of 3000 μm (see Table 1) within this time. The longer a particle remains in the respiratory system,

Table 1 Mean Displacement of Unit-Density Spheres in 1 s by Gravitational, Inertial, and Diffusional Transport

Diameter (μm)	Settling distance (μm)	Stopping distance (μm)	Diffusional displacement (μm)	Mass (pg)
25.0	18,203.3	1,892.5	1.46	8,181.2
10.0	2,912.9	3,02.8	2.32	523.4
5.0	739.9	75.7	3.30	65.45
2.0	124.0	12.1	5.34	4.19
1.0	33.34	3.02	7.84	0.524
0.5	9.54	0.76	11.85	6.545×10^{-2}
0.2	2.19	0.12	22.31	4.189×10^{-3}
0.1	0.87	0.03	39.19	5.236×10^{-4}
0.05	0.38	0.008	72.96	6.545×10^{-5}
0.02	0.144	0.001	174.53	4.189×10^{-6}
0.01	0.071	0.0003	343.96	5.236×10^{-7}

Temperature: 37°C; atmospheric pressure 1013 hPa, viscosity: 1.9×10^{-5} Pas, stopping distance is given for particles with an initial velocity of 1 m s^{-1}, mass is given per particle.

the larger is the settling distance the particle will cover and, hence, the probability that the particle will touch airspace walls. Therefore, the relative long residence time in the small conducting airways and in the gas-exchanging region of the lung will favor particle deposition by gravitational sedimentation.

Impaction. Inertia is the inherent property of a moving mass to resist accelerations. It may cause particles to continue to move in their original direction and not follow airflow streamlines, such that they deposit on airway walls by impaction (see Fig. 3). The inertia of a particle depends not only on the particle density and the particle diameter, but also, in contrast with gravitational settling and diffusional displacement, on the airflow velocity. A unit-density sphere of 1-μm diameter, traveling with a velocity of 1 or 5 m s^{-1}—which are typical airflow velocities prevailing in the larger conducting airways during quiet breathing and during moderate exercise—stops within a distance of 3 or 15 μm on a sudden cessation of airflow, whereas a unit-density 10-μm sphere continues to travel for 300 or 1500 μm (see Table 1). Inertial impaction will most likely occur in the extrathoracic airways and in the large conducting airways of the lung, where flow velocities are high and rapid changes in airflow direction occur.

In the light of the transport mechanisms causing particle deposition in the respiratory system, the dependency of total deposition on particle diameter, as displayed in Figure 1A, becomes clear. Minimal deposition occurs in the size range between 0.1 and 1 μm, because neither impaction or sedimentation nor diffusion are effective in particle displacement. With decreasing particle diameter, diffusional particle displacement increases so that particle deposition in the respiratory system increases. With increasing particle diameter, the distance covered by sedimentation or impaction increases such that total particle deposition is also enhanced.

In how far do physical particle features determine regional particle deposition? During quiet breathing, inertial impaction appears to be negligible for particles smaller than 2 μm (see Fig. 1B–D), so that those particles escape deposition within the extrathoracic region and the large conducting airways, but they are collected by the time-dependent deposition mechanisms—diffusion and sedimentation—in the small conducting airways and the alveolar region of the lung. Conversely, large particles, with a diameter of about 10 μm, are most likely deposited by impaction in the extrathoracic region, so that only some particles reach the large conducting airways, where they are also deposited by impaction. With decreasing particle diameter, particle displacement by inertia decreases, so that more and more particles escape deposition in the extrathoracic and the large conducting airways. They are caught in the small conducting airways or even in the alveolar region of the lung, either by sedimentation or by diffusion.

Particle Deposition Related to Breathing Patterns. An increase in tidal volume, while keeping the flow rate constant, will transport particles by convection deeper into the lung and increase their mean residence time in the lung.

Hence, more particles reach smaller, peripheral lung structures and more time is available for gravitational and diffusional particle transport. Therefore, an increase in total deposition is found for all particle sizes (see Fig. 2). On the other hand, keeping the tidal volume constant while increasing flow rate enhances total particle deposition for particles larger than 2 μm, but decreases total deposition of smaller particles. This is because the higher flow rate increases the probability for particle losses by impaction in the extrathoracic and large conducting airways, but particle losses by diffusion and sedimentation are decreased because of the shorter available time for deposition.

In summary, deposition occurs solely in alveolated airspaces for particles of minimum deposition. With decreasing and increasing particle size, the site of deposition shifts from distal to proximal airspaces. Consequently, targeting of specific airspaces in the lung with particles is possible if an appropriate particle size is chosen. This targeting can even be improved by making use of appropriate breathing patterns. Details are presented in the following paragraphs.

II. Basics and Definitions

A. Aerosol

An *aerosol* is a suspension of particulate matter in air. It comprises airborne droplets, solid particles, or both; all will be referred to as "particles" in this paper. Because of mechanical particle transport, an aerosol is intrinsically unstable (i.e., particles tend to deposit onto exposed surfaces); also, small aerosol particles at high concentrations tend to aggregate.

Physical Description of an Aerosol

Particle Diameters

Most aerosols are heterodisperse, possibly containing particles of varying sizes, shapes, and densities. The physical description of an heterodisperse aerosol may be misleading if simple geometric terms are used for particle characterization (e.g., the *geometric particle diameter, d*). Hence, equivalent particle diameters related to distinct physical particle properties are often applied. For example, particles may be classified relative to their gravitational settling, and compared by their *aerodynamic diameter* d_{ae}, where d_{ae} is the geometric diameter of a unit-density sphere that has the same gravitational settling velocity as the particle in question. Accordingly, equivalent diameters may be based on particle inertia, or they may be related to diffusional transport (*thermodynamic diameter*, d_{th}). But the light-scattering properties of particles are also applied for classification.

The particle diameters given in this paper refer to the geometric diameter of a unit-density sphere, if not otherwise specified.

Particle Size Distribution

Most frequently, an aerosol is characterized by its particle size distribution. Usually this distribution is reasonably well approximated by a log-normal frequency function (Fig. 4A). If the distribution is based on the logarithm of the particle size, the skewed log-normal distribution is transferred into the bell-shaped, gaussian error curve (see Fig. 4B). Consequently, two parameters are required to describe the particle size distribution of an aerosol: the *median particle diameter* (MD), and an index of dispersion, the *geometric standard deviation* (σ_g). The MD of the log-normal frequency distribution is equivalent to the logarithmic mean and represents the 50% size cut of the distribution. The geometric standard deviation is derived from the cumulative distribution (see Fig. 4C) by

$$\sigma_g = \sqrt{\frac{d_{84}}{d_{16}}} \tag{1}$$

where d_{16} and d_{84} are the particle diameters at the 16 and at the 84% size cut of the distribution. Depending on the biological effect under consideration, the particle size distribution of an aerosol may be related to the number of particles, currently discussed as an important factor for effects of ambient ultrafine particles. Alternatively, it may be related to the mass of particles; for instance, for therapeutic aerosols, for which the mass delivered to the respiratory system is of significance. For particles absorbing toxic constitutes onto their surfaces, the surface area of the particles is the appropriate parameter. Accordingly, the size distribution may be described by the *count median diameter* (CMD), the *mass median diameter* (MMD), or the *surface median diameter* (SMD). The count, the mass, or the surface distribution, all exhibit the same geometric standard deviation, and a clear relation between the means is given, in that CMD is smaller than MMD, whereas SMD is always in-between (see Fig. 4).

Monodisperse–Polydisperse Aerosols

If all particles of an aerosol are of uniform size, an aerosol is termed *monodisperse*. Because in reality perfect monodispersity does not exist, an aerosol is termed monodisperse if the geometric standard deviation of the particle distribution is smaller than 1.2. For deposition analyses, all particles of a monodisperse aerosol are considered to behave as if they had exactly the same diameter as the MD of the size distribution. In *polydisperse* aerosols, particles of widely differing sizes are present, and σ_g is larger than 1.2.

Particle Classes

The upper limit of diameter for respirable particles is approximately 50 μm in humans, but differs among species (6–9). According to their diameter, particles are commonly grouped into different classes: ultrafine, fine, and coarse particles.

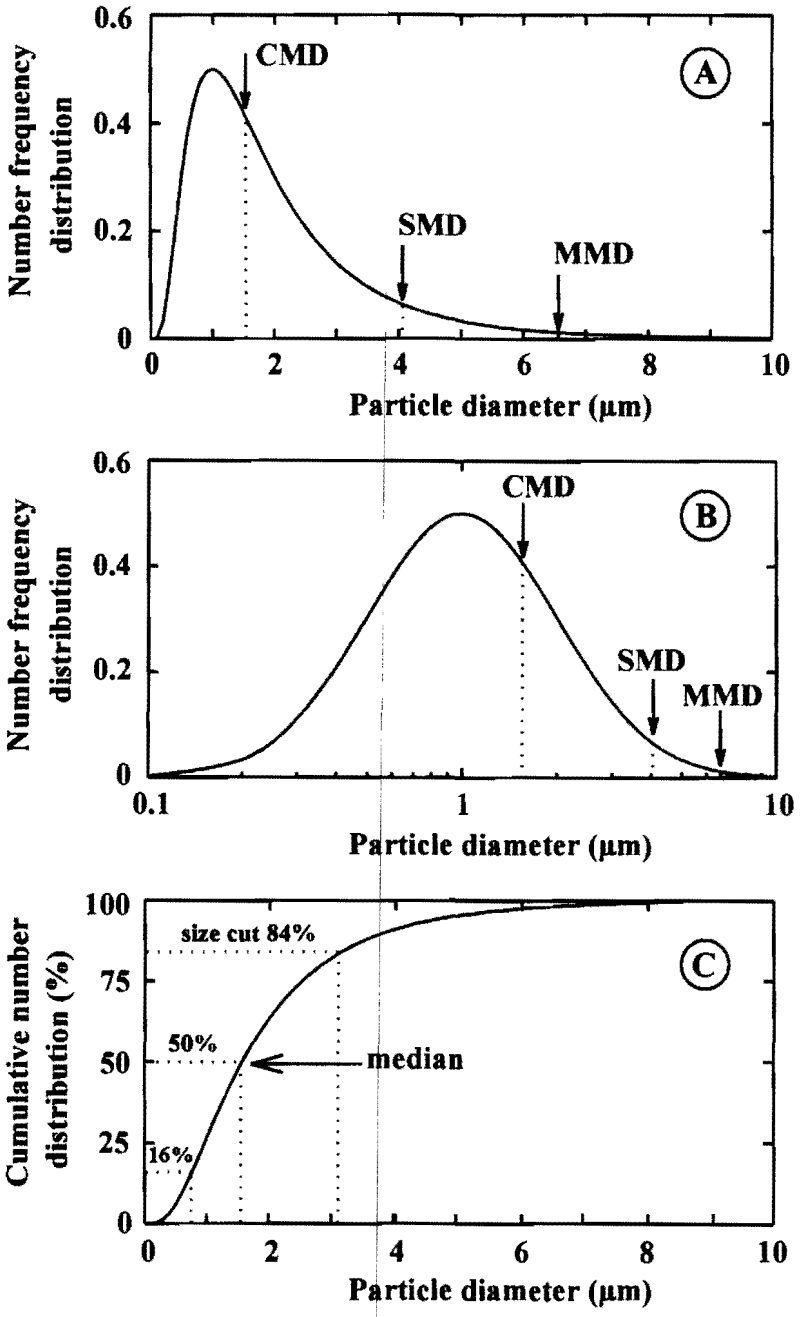

Figure 4 (A, B) Number-frequency distribution and (C) cumulative number distribution of an aerosol of unit-density spheres. Indicated are the count median diameter (CMD), the surface median diameter (SMD), and the mass median diameter (MMD) of the number-frequency distribution. The 16, 50, and 84% size cut of the cumulative number distribution are shown. For further explanation, see text.

Particles smaller than 0.1 μm in diameter are frequently called *ultrafine particles*. The definitions given for fine and coarse particles differ. The Environmental Protection Agency (EPA) convention, originally intended to apply to the two major atmospheric particle distributions, defines particles in the size range between 0.1 and 2.5 μm as *fine particles*, and those larger than 2.5 μm in diameter as *coarse particles*. According to the Health Effects Institute (HEI) convention, particles with diameters between 0.1 and 1 μm are *fine particles*, whereas *coarse particles* are larger than 1 μm in diameter.

In physical terms, particles are classified into different domains relative to their predominant mechanism of mechanical particle transport. Particles smaller than 0.1 μm are related to the *thermodynamic domain* and particles larger than 1 μm to the *aerodynamic domain*. A *transitional domain* is defined for those particles with diameters between 0.1 and 1 μm (10). A detailed overview of the different particle classifications is given in Chapter 1.

B. Deposition

In a mathematical sense, deposition refers to the mean probability for an inspired particle to be caught in the respiratory system. It is derived from particle number or mass balance considerations over a given respired volume, a given number of breaths, or a given time period. Deposition occurs when particles strike the wet airspace surfaces of the respiratory tract, but it also takes place when convective mixing of inhaled with reserve air causes particles not to be recovered on subsequent expirations. The site of initial particle contact with the airspace surface is considered the *site of initial deposition*. Thereafter, particles may rapidly be dislocated by means of mucociliary clearance or by macrophages after phagocytosis (11; see also Chap. 7).

Total, Regional, and Local Particle Deposition

Total deposition fraction or *total deposition* is the fraction of inhaled particles deposited in the entire respiratory system. Total deposition is composed of the sum of regional depositions taking place within distinct regions of the respiratory tract. Two main regions are considered: the extra- and intrathoracic regions. Deposition in the *extrathoracic region* refers to deposition occurring in the nasopharyngeal or oropharyngeal airways and the larynx during nose or mouth breathing. It was previously considered as *laryngeal deposition*, for mouth breathing or *nasopharyngeal deposition*, for nose breathing. *Intrathoracic deposition* is given by the quantity deposited in the *tracheobronchiolar region* (corresponding to the bronchial and bronchiolar region [BB + bb] of the ICRP model; see 138) and in the *alveolar region*.

Particle collection on a subregional level is defined as *local deposition*. For example, local deposition in the nose may refer to deposition occurring in the

nasal valve, the nasal mucosa covered with hair, or the turbinated area of the nose. Local deposition also refers to deposition occurring in certain airway generations within the tracheobronchiolar tree.

III. Physical Mechanisms of Particle Deposition in the Respiratory Tract

Particle deposition in the respiratory system is related to distinct physical mechanisms operating on inhaled particles. The most important of these mechanisms are gravitational sedimentation, impaction by inertial forces, and brownian diffusion (see Fig. 3). Electrostatic forces and interception, the latter being significant only for fibers, are generally less important. In this section the physical mechanisms are briefly introduced. Several excellent overviews are available in the literature (12–14).

A. Gravitational Sedimentation

Particles are continuously exposed to gravity and undergo gravitational settling in air. During sedimentation, a particle acquires its terminal settling velocity v when gravitational forces are balanced by viscous resistive forces of the gas. This is described by *Stokes' law*, given here for a spherical particle with geometric diameter d and density ρ

$$\left(\frac{\pi}{6}\right) \rho\, d^3\, g = 3\,\pi\,\eta\, d\, v \tag{2}$$

The force of gravity on the particle is characterized by the left-hand side of the equation, where g is the gravitational constant. The right-hand side represents the resistive forces, where η is the dynamic viscosity of the surrounding medium. For the size region smaller than 1-μm diameter, the *Cunningham slip correction factor* (C_s; 15) has to be applied to take the discontinuity of the surrounding medium into consideration. This results in a higher settling velocity than predicted by Stokes' law. The *terminal settling velocity* for spherical particles is then

$$v = \frac{\rho\, d^2\, g\, C_s}{18\,\eta} \tag{3}$$

Settling velocities for particles of different sizes are given in Table 1. Gravitational particle displacement becomes more effective than diffusional displacement for spheres larger than 0.5 μm.

Respirable particles acquire this terminal settling velocity in less than 0.1 ms (13), a fraction of less than 1% of the typical transit time of the airflow in any airway generation of the bronchial tree. For all practical purposes, therefore,

particles may be considered to reach their terminal settling velocity instantaneously.

The probability of a particle for depositing on airway walls by gravitational settling is proportional to the distance a particle will cover within the airways; hence, it is proportional to the square of the particle diameter. The *settling distance* in the respiratory system is determined by v times the particle's residence time (t_{rs}). Breath-holding at the end of inspiration increases gravitational deposition, for the residence time and, hence, the settling distance is increased. Considering the respiratory flow rate Q, gravitational deposition is proportional to the parameter d^2/Q.

The efficiency of gravitational deposition is higher in tranquil than in stirred air (16), where particle settling is superimposed on components of convective transport. Convection may move particles back into volume elements previously cleared by gravitational settling. During stirred settling, particle concentration reaches $1/e$ times the original concentration in the same time that is required for complete removal of particles from tranquil air (13).

B. Inertial Impaction

The particle's inertia is related to its momentum (i.e., to the product of the particle's mass and its velocity). A particle's inertia can be assessed by the stopping distance (i.e., by the distance a particle with a given initial velocity will travel in still air in the absence of external forces). Table 1 shows stopping distances of particles traveling with a velocity of 1 m s^{-1}, a typical linear airflow velocity prevailing in the first ten airway generations of the bronchial tree during quiet breathing. It appears that inertial displacement becomes significant during quiet breathing for particles larger than 2 μm.

The likelihood that spheres with the diameter d and density ρ moving in an airstream with linear velocity u will diverge from airflow streamlines is characterized by the dimensionless *Stokes' number* (Stk)

$$\text{Stk} = \frac{\rho\, d^2\, u}{18\, \eta\, G} \tag{4}$$

where G characterizes the geometry of the structure in which particles are traveling (e.g., the diameter of a tube). The higher the Stokes' number, the more readily particles will depart from airflow streamlines, and the more likely they are to be deposited by inertial impaction on airway walls. For respiratory flow rate Q, inertial deposition in a given geometric structure is proportional to the *impaction parameter* d^2Q.

C. Brownian Displacement

Gas molecules are in constant motion because of their thermal energy. The mean free path λ traveled by a molecule in air between successive collisions with other

gas molecules is about 0.07 μm under ordinary atmospheric conditions (i.e., about 150 times the molecular diameter). The speed of the gas molecules is about 100 m s^{-1}, leading to a collision frequency of about 5×10^9 s^{-1} (13,17).

For particles with a diameter close to λ, collisions with gas molecules can be considered as discrete events, causing an irregular, wiggling motion of the particle (see Fig. 3). With increasing particle diameter, the number of collisions occurring at one time from different directions increases, such that particle displacement, as the net result of all momentums applied, in effect, is reduced. Mathematically, particle transport by brownian motion is characterized by the *diffusion coefficient* D_P. For a spherical particle with the diameter d, D_P is given by

$$D_P = \frac{\kappa T C_s}{3 \pi \eta d} \tag{5}$$

where η is the viscosity of the surrounding medium, C_s is the slip correction factor, T is the absolute temperature, and κ is the Boltzmann constant. Unlike gravitational displacement or impaction, diffusional transport is independent of particle density, but also depends on particle shape (18,19). The *root mean square diffusional particle displacement* Δ for particulate matter subjected to stochastic transport processes (20)

$$\Delta = \sqrt{2 D_P t} \tag{6}$$

is given for $t = 1$ s in Table 1 for particles of different sizes. Diffusional displacement becomes effective for spheres smaller than 0.5 μm.

The probability for a particle to be deposited by diffusional displacement increases with $(t_{rs}/d)^{1/2}$, where t_{rs} is the residence time in the respiratory system. For the respiratory flow rate, diffusional deposition is a function of the *diffusion parameter* D_P/Q.

D. Interception

Interception takes place when a particle is brought close enough to the airway surface that an edge contacts the surface. Interception is usually important only for fibrous particles, such as asbestos fibers, because deposition by interception requires that the particle size is a significant fraction of the airway diameter. The aerodynamic diameter of fibers is predominantly determined by their geometric diameter and is about three times the fiber diameter, if the length/diameter ratio is larger than 10 (21–23). Hence, a fiber with a diameter of 0.5 μm and a length of 100 μm behaves the same as a 1.5-μm sphere in terms of sedimentation and impaction. Therefore, fibers have a low probability of deposition in the conducting airways by impaction or sedimentation, but interception has to be considered as an important mechanism.

E. Electrostatic Forces

Most ambient particles become neutralized naturally by air ions, but many freshly generated particles are electrically charged. The level of charge may vary widely, depending on the nature of the material, the mode of mechanical generation, and the age of the particles. Charged particles may have an enhanced deposition. For low particle–number concentrations ($< 10^5$ cm^{-3}), deposition increase is assumed to result from the electrostatic image charges generated on the surface of the airways by the charged particles (24). A threshold charge is required to enhance deposition, which Yu (24) found to be about 50 elementary charges for 1-μm particles. For each particle size, deposition increases linearly with the number of elementary charges prevalent on the particles. Electrostatic forces may increase deposition up to a factor of 2, but generally deposition is influenced to a lesser extent, by only about 10% (24–29).

IV. Methods of Assessing Particle Deposition in the Respiratory Tract

A. Experimental Approaches

Noninvasive Techniques

Radioactivity

Radioactive aerosols are frequently used in deposition or medical application studies because they allow noninvasive measurements of high sensitivity and reasonable spatial resolution. The fraction of aerosols deposited in the body is derived from radioactivity balance considerations.

Inhaled particles can be labeled with a variety of radionuclides, emitting β-rays or γ-rays. The β-rays are highly absorbed from tissue, so that they are almost undetectable from outside the body. With β-emitting radionuclides (e.g., ^{3}H or ^{14}C), particle deposition in the respiratory system or in the mouth can be assessed only from radioactivity recovered on expired-air filters or in lavage fluid from mouth washings.

As body tissues are much more radiolucent for γ-rays, γ-labels can provide information on the amount and the distribution of particles deposited in the respiratory system by using external radioactivity counts. Total deposition is inferred from the activity present in the entire body, whereas regional deposition is assessed from the radioactivity measured over the extrathoracic and the intrathoracic regions. Beside the spatial resolution of γ-count images, time kinetics of particle clearance are commonly used to further separate intrathoracic deposition into tracheobronchiolar and alveolar deposition: Fast-cleared activity is assumed to have been deposited in the tracheobronchiolar region, whereas that cleared slowly is assigned to the alveolated regions of the lung. This functional separa-

tion, however, has become a matter of controversial discussion because recent experimental results suggest that a significant fraction of particles deposited in the tracheobronchiolar region is retained much longer than previously assumed (30–32; see also Chap. 7).

Despite continuous technical improvements, deposition measurements based on external γ-counts still suffer some limitations from image nonuniformity, spatial resolution, detection efficiency, and counting linearity (33–35). Gamma rays that originate from different regions of the lungs as well as from the stomach or from the head are attenuated and scattered to variable degrees during their passage through the tissues. Hence, for a reliable interpretation of external γ-counts, it is necessary to apply suitable attenuation factors for different regions of the body. However, these factors can vary by a factor of 5 between subjects, and the use of individual corrections has been recommended for precise deposition measurements (36–43).

For stable γ-labeling of inhaled aerosols, different radioisotopes (e.g., ^{11}C, ^{57}Co, ^{60}Co, ^{67}Ga, ^{111}In, or ^{99m}Tc) are available, providing a wide spectrum of energies, types of radiation, half-lives, and doses. Unfortunately, it is technically difficult to label pharmaceutical agents directly, so that in most medical deposition studies a surrogate of radiolabeled particles or a mixture of drug substance and labeled particles is employed.

Devices Detecting Emitted γ-Rays. The total amount of material deposited in a subject after exposure to a γ-tagged aerosol can be determined in a *whole-body counter*. The energies of γ-quanta are measured by registration of the light pulses they produce in a sodium iodide crystal. Whole-body counters may use only one detector surrounding the subject completely (44), or several smaller detectors (40,45,46). Improved systems employ a *collimator*, which works like a lens and restricts the field of vision of the detector to a certain region of interest (e.g., to the extra- or the intrathoracic regions; 42,47,48). The amount of radioactivity to be detected by a whole-body counter can be small, a typically administered activity is approximately 0.01 MBq.

The *scintillation gamma camera*, developed by Anger in 1953, uses a single, large planar scintillation crystal masked with a honeycomb lead collimator containing as many as 15,000 parallel holes. The scintillations in each element of the crystal are elicited by incoming γ-rays, projected from only a small area of the body. They are sensed by phototubes, and the signals are converted to a two-dimensional radioactivity image reflecting the deposition pattern within the respiratory system. However, only limited information is given about the anatomical location of particles deposited within the lungs. A variety of indices calculated to quantify the deposition pattern in central and peripheral lung structures, among which the "penetration index" is most frequently used, implies that the central regions of the thoracic image represent mostly the large conducting airways (e.g., 33,49–54). However, in three-dimensional space, the presence of

small airways and alveoli overlying the central airways within the thorax must be taken into account and precludes a precise separation of materials deposited in these physiologically and anatomically distinct regions (38,50). Radioactivity administered for gamma-camera imaging typically ranges between 2 and 10 MBq.

Three-dimensional images of the distribution of radioactivity in the thorax are obtained by *tomographic emission scanners* (36,37,54,55), using one- or multiple-headed cameras that are rotated along different planes around the source organ. By computational techniques a three-dimensional view of the radionuclide distribution is constructed. Spatial resolution is sufficient to estimate particle deposition in the largest conducting airways, but not in the smaller structures. Tomographic emission scanners are not indicated for total deposition studies, because long patient examination times and large quantities of radioactivity (25 MBq) are needed, and anteroposterior (AP) planar imaging is capable of providing information on total deposition with a similar accuracy (36).

Magnetopneumography

Magnetopneumography was developed by Cohen in 1973 (57) and was used in occupational exposure studies to estimate the quantity of magnetizable mineral dusts in the lungs of welders, coal or asbestos miners, and dental technicians (56–60). The technique consists of applying a magnetic field to the whole thorax or to localized areas and measuring the remanent magnetic field of retained lung particles by sensitive magnetometers. With a calibrated system, the magnitude of the magnetic field gives the amount of accumulated magnetic particles in the respiratory system. In deposition studies on volunteers, magnetide (Fe_3O_4) or hematite (γ-Fe_2O_3) particles have been applied (61,62). Disturbingly, the magnitude of the remanent magnetic field increases in the first days after inhalation. Redistribution of dipole magnetic particles in the lung periphery associated with alveolar macrophage motility is considered to be responsible for this phenomenon (60,63,64). It precludes a reasonable interpretation of magnetometric deposition data to date.

Light-Scattering Photometry (Tyndallometry)

The light-scattering technique enabled Tyndall in 1881 (65), for the first time, to directly observe that inhaled particles are retained in human lungs. Decades later, Altshuler and co-workers (66) were the first to apply this technique for the quantification of total particle deposition in human lungs. Since then, tyndallometry has been used in numerous deposition studies (e.g., 67–75).

Tyndallometry is based on the measurement of the intensity of light scattered by inspired and expired particles while they pass through a light beam close to the entrance of the respiratory system. The scattered light originates from all particles simultaneously present in the beam. Its intensity depends on particle number concentration, but also on diameter and refractive index of the aerosol

particles. In applying nonhygroscopic, monodisperse particles, the intensity of the scattered light is solely proportional to particle number concentration. When light-scattering photometry is combined with pneumotachography, a continuous monitoring of particle number concentration in the respired air, as a function of the respired volume, is possible. Total deposition is given by

$$DE_{\mathrm{Tot}} = 1 - \frac{\int_{V_{\mathrm{ex}}} C(V)\, dV}{\int_{V_{\mathrm{in}}} C(V)\, dV} \tag{7}$$

where V_{in} and V_{ex} are the inspired and expired volumes and $C(V)$ is the corresponding particle number concentration. Currently, this technique is introduced as a "respiratory aerosol probe" into clinical studies (76). It can be used to gain not only total deposition, but also particle deposition in so-called volumetric lung compartments (67,77,78). For that purpose, the inspired volume is considered as a succession of many small volume elements. Elements inspired at the onset of inspiration penetrate deeply into the respiratory system, those inspired at the end of inspiration penetrate much less. When a single volume element is labeled with particles, an aerosol bolus is inspired. If particle deposition is determined from a series of boluses inhaled into different volumetric lung regions—"series bolus delivery technique"—a simple algorithm can be used to estimate deposition in these volumetric compartments (67). In that case, the lung region is characterized by the volume of respired air transporting the particle bolus convectively into the respiratory system. Model simulations have to be used in a second step to convert volumetric lung regions to distinct anatomical regions (e.g., to the alveolated region or to the conducting airways).

Invasive Techniques

Postmortem measurements in laboratory animals supply information about regional or local deposition patterns in the lungs at better spatial resolution than noninvasive techniques can provide. Most frequently, radioactively labeled particles are applied, but magnetically labeled particles, microspheres, or fluorescent particles have also been used to quantify deposition throughout the lung on a macroscopic or microscopic level (79). Most of the invasive techniques require special lung fixation procedures before retention analysis to avoid translocation or particle loss during the fixation procedure (11,74). Rapid microwave fixation (80–82), intravascular perfusion techniques (74,83), and cryofixation (84) have been applied (see also Chap. 6).

Measurement Techniques

No single technique can provide all possible information on intrapulmonary particle deposition, so that the choice of the technique clearly depends on the question to be answered.

Lung or lobe dissection provides estimates about regional particle deposition on a macroscopic scale. Lobe-to-lobe, apex-to-base, or ventral-to-dorsal differences can be assessed. *Piece dissection* is used to estimate overall deposition heterogeneity throughout the lung or within a lung region. Regions with a high or a low particle load can be identified (80,85,86). The next level of detail is provided by *autoradiographs* (81,86–89). Thin lung slices are placed in direct contact with x-ray films and a crisp image of the distribution of radioactivity over the surface of the slice is obtained. With an overlay tracing of the lung slice, particle distribution can be mapped in detail. Quantitative information is obtained by computer-assisted correlation of anatomical features with the film density (89).

Unbiased stereological sampling techniques in combination with morphometrical analysis are required to obtain information about how particles are distributed throughout distinct anatomical compartments of the lung (e.g., respiratory bronchioles or alveolar ducts, 90–93; see also Chap. 6). This type of approach can also provide information about the dose of particles per surface area retained in the various compartments of the lung. In combination with confocal microscopy, the anatomical site of particle deposition can be examined in three dimensions (Fig. 5; 83,84).

To localize particles or soluble remanents of particles within cells or on the level of subcellular compartments, electron microscopic techniques are necessary (i.e., *electron spectroscopic imaging* and *electron energy loss spectroscopy*; 95,96).

Deposition in Physical Models

Experimental studies in idealized bronchial structures (e.g., 97–103) or in replicates of casts (e.g., 104–112) allow "inhalation" of substantial amounts of particles into easily accessible structures without having to deal with secondary redistribution phenomena caused by continuous particle clearing or lung preparation processes. They are performed to obtain information on primary deposition patterns with finer spatial resolution than is possible in in vivo experiments. These types of measurements may also be considered as the experimental match, validating theoretical approaches on particle deposition (see later). Mean local deposition rates, but also the heterogeneity of particle deposition within bifurcating zones, were investigated. Many studies (98–103,105,111) specifically focused on localization of so-called hot-spots, which are sites of enhanced deposition within the larynx or the tracheobronchiolar tree and may be most important rela-

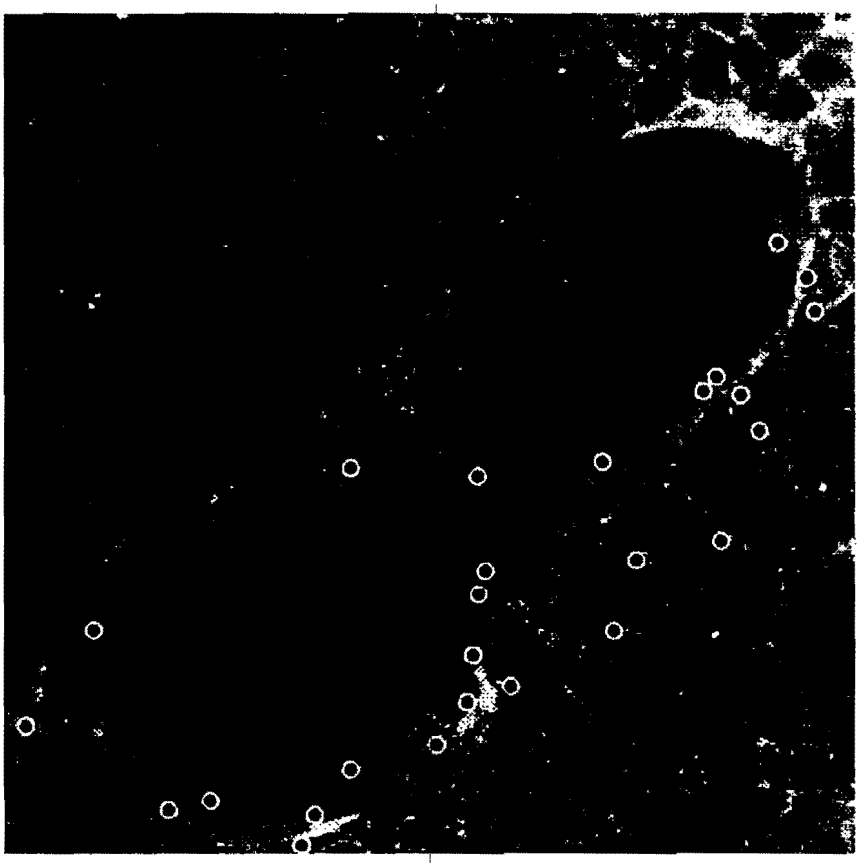

Figure 5 Sites of particle deposition assessed by confocal microscopy. Deposition sites of red and green fluorescent particles with a diameter of 2 μm are shown in a bifurcation of a canine bronchiole surrounded by lung parenchyma. Please note, particles are marked with a thin white circle to improve their appearance in this black and white copy.

tive to human health hazards arising from airborne particles. To a lesser extent, the influence of specific airflow fields on the pattern of intrabronchial deposition has been studied (98,99). In models of single bifurcations or of few successive airway generations, structural parameters of bifurcations (e.g., branching angles or symmetry) were varied systematically to evaluate factors governing the process of deposition within these model bifurcations (98,99,103).

Limitations arise particularly when studies are performed in idealized tubular structures, because geometric features of the conducting airways are simplified to an extent that may result in unrealistic airflow fields and unreasonable particle deposition patterns. Replicates of bronchial casts provide a more realistic flow geometry. Often constant airflows are used, which to some extent can only mimic the effects of in vivo flow variations. Little information is available, however,

on whether particle deposition patterns resulting from constant-flow inspirations are the same as those resulting from variable-flow inspirations.

B. Model Simulations

Mathematical Models

In the last decades, various mathematical approaches have been introduced to predict the amount, the anatomical sites, and the underlying mechanisms of particle deposition in the respiratory system. Modeling particle deposition requires idealized assumptions about the structure of the respiratory system (morphometric model), the particle transport through the airways (gas dynamics model) and toward the airway surfaces (mechanical particle transport model), and about the physiological parameters characterizing breathing patterns (physiological model). Having chosen an appropriate set of assumptions, the physical laws of mass, heat, and momentum conservation are employed to quantify the dynamics of interest and to determine their effect on particle deposition. Depending on the method and the degree of idealization, there are many different ways to create deposition models, and there is ample work on this subject available in the literature (113–116). Regardless of the approach chosen, all models published so far were capable of characterizing deposition in the respiratory system reasonably well in comparison with existing experimental data.

The models introduced by Findeisen (117), Altshuler (118), and Taulbee and Yu (119) are considered "primary deposition models," in that each proposed original and independent mathematical formalisms to describe particle transport onto airway surfaces. Incidently, they are also based on different models of the geometric structure of the human lung. Later, the formalisms of the primary models were adopted and modified by many authors, resulting in so-called "secondary deposition models" (120–134). Recent models have been proposed by the U.S. National Council on Radiation Protection and Measurements (NCRP; 136–137) and by the Task Group on Human Respiratory Tract Models for Radiological Protection (ICRP; 137,138).

In 1935, the meteorologist Findeisen was the first to introduce a lung deposition model. The geometric structure of the lung is treated as a system of nine regions, arranged in series and characterized according to the functional and anatomical features of different-sized airway structures. The model neglects extrathoracic airways and starts with the trachea, the last region contains the alveolar sacs. Particle transport through airways occurs solely by convective bulk flow, whereas mixing processes are neglected. Particle loss onto airway surfaces is considered as a function of impaction, sedimentation, and diffusion, which are assumed to act independently of each other. Findeisen's estimations of total thoracic particle loss for the size range between 0.03 and 10 μm are shown in Figure

6. Interestingly, despite the relative simplicity of his model, subsequent, more sophisticated models, as well as experimental data, in principle, confirmed his predictions. This holds true for modifications of the Findeisen model by Landahl (121,122), who added a region representing mouth and pharynx, and by Beeckmans (123,124), who further considered convective mixing in particle transport processes. The first international attempt to assess regional particle deposition in the lung was based on the Findeisen–Landahl–Beeckman modeling (126).

In contrast to Findeisen's approach, the model proposed by Altshuler (118) is spatially continuous, in that the entire respiratory tract is considered a continuous filter bed. Altshuler's model was not adopted by other authors, but applied in several studies of his own group (139,140).

Taulbee and Yu (119) developed a formalism to assess particle number concentration in the human lung at any lung depth and any time during the breathing cycle, so that their model is spatially and temporally continuous and allows the simulation of arbitrary breathing conditions. The applied gas dynamics model

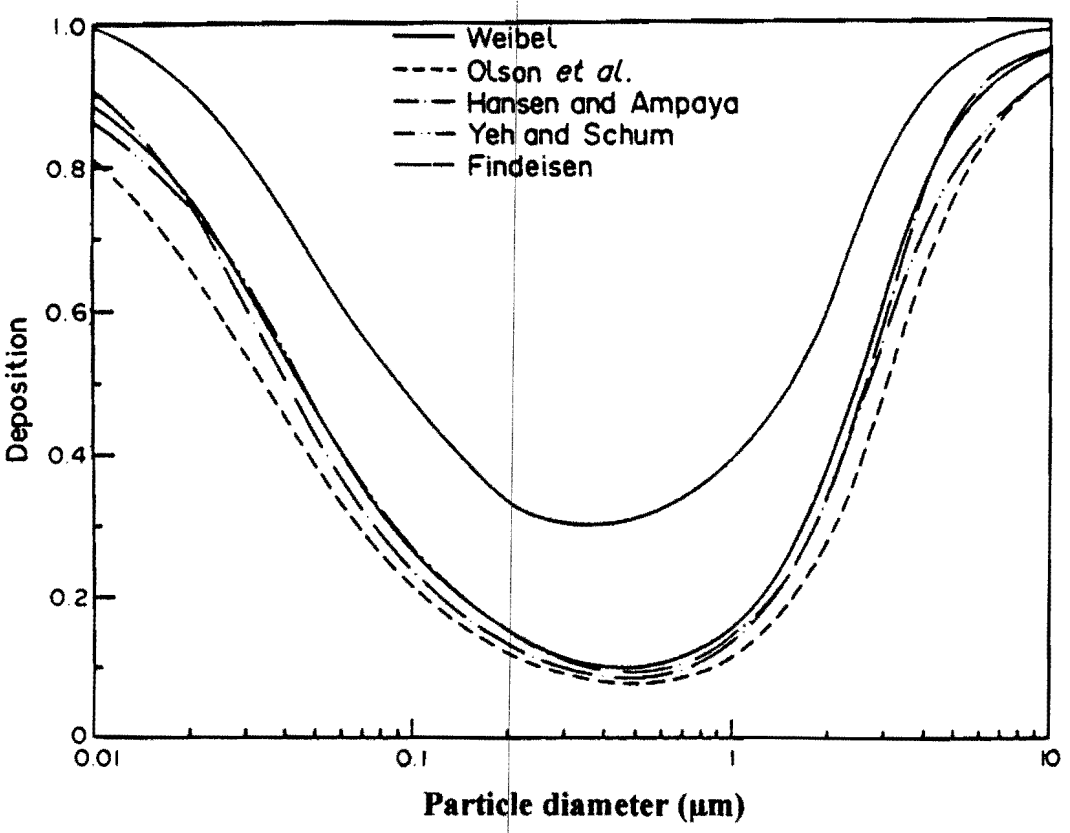

Figure 6 Total deposition fraction of unit-density spheres during mouth breathing: Data were modeled for a tidal volume of 1000 cm^3 and a rate of 15 breaths per minute and for different morphometric models of the human lung. (From Ref. 150.)

considers longitudinal mixing in conducting airways and convective mixing between inhaled and residual air in alveolated airways. The morphometrical model approximates the many generations of the airways by a trumpet-shaped structure, with a variable, continuously increasing cross section along its depth.

This "trumpet model" was originally introduced by Scherer et al. (141) for simulations of intrapulmonary gas transport and is based on a morphometric data set proposed by Weibel (5). In Weibel's model, the structural parameters of each airway generation are described by average values, so that all airways of a given generation are identical, as are all pathways leading to a specific airway generation. The model is, therefore, termed "symmetrical" or "deterministic."

Most of the later proposed secondary deposition models use symmetrical morphometric model structures (e.g., 121,125,127–129,144), whereas some others are based on a system of asymmetrically branching airways (e.g., 130,132–134,145–147). Various simulations neglect the existence of alveoli, whereas others add all the alveoli to the last airway generation or add increasing numbers of alveoli to consecutive airway generations within an acinus. However, the influence of using different morphometric data sets is small, and calculated total or regional deposition does not vary considerably from one model to another (see Fig. 6; 115,148–150).

A so-called stochastic airway model was proposed by Koblinger and Hofmann (146,147). It is based on statistical relations (evaluated on airway casts) between geometrical parameters of a given parent airway and those of the two branching daughter airways. This model shows a significant variability of airway lengths, diameters, and numbers of airway generations along different pathways. The transport of inspired particles occurs by randomly selecting at each bifurcation the sequence of airways an individual particle is passing through. Interestingly, the effect on calculated total or regional deposition again appears to be minor when compared with other lung models. However, within the intrathoracic airways, deposition appears to be partially shifted to more distal airways. Furthermore, this model may provide insight into the deposition variability potentially present in the lung within airways of a given generation (115,133,134,147).

All of the foregoing deposition models are based on the assumption of uniform particle distribution within and among airways. However, local deposition per unit surface area is frequently important for the assessment of possible risks from ambient air pollution, and local accumulations of particles can occur in bifurcating systems. Nowadays, computational techniques and capacities allow theoretical deposition models to focus on local particle deposition in subunits of the respiratory system (e.g., in the oropharyngeal cavity) or in three-dimensional airway bifurcation models. Air velocity fields are computed by numerical modeling techniques solving the Navier–Stokes equation in the respective model geometry (151–158). Particles are then virtually entrained in the airstream, and particle trajectories are simulated by solving the equations for particle motion. Local par-

ticle deposition patterns within the three-dimensional model are inferred from the intersection of particle trajectories with the adjacent model surfaces. So far, the effects of asymmetries in airway diameters, branching angles, or flow division, and the influence of the gravitational angle at bifurcations have been studied in idealized airway models. Recently, a new approach was introduced by Perzl et al. (159) to make real-lung geometries available for computational deposition modeling. Two-dimensional images of a canine cast obtained by high-resolution computed tomography were combined to yield a three-dimensional volume data set. After image processing, a three-dimensional polygonial surface representation from the cast was created, showing excellent conformity with the original cast. Based on this surface representation, a finite-element mesh was generated, allowing computational fluid dynamics in realistic conducting airway structures (160). These numerically modeled airflow fields can even be verified in hollow replicates of these computational surface representations by measuring experimentally the flow fields applying the laser-light-sheet imaging method (161,162).

Empirical Models

A different approach to deposition modeling is the empirical one, in which semiempirical functions, derived from experiments or theory, are developed to quantify deposition for a wide range of particle sizes and breathing conditions. The empirical models consider the respiratory system to be a series of filters representing the various anatomical or functional regions of the system. Parameters characterizing particle motion by impaction, sedimentation, and diffusion are developed, and the dependence on the filtration efficiencies of the respective regions is determined. By means of the least-square method, the parameters are optimized to fit experimental data (112,163–168). An advantage of this type of modeling is that it presents relatively clear-cut algebraic approximations that provide qualified estimates of regional particle deposition. It also represents a tool for interpolating and extrapolating missing experimental data on a simple basis.

V. Total Deposition

Numerous studies have investigated total deposition in human lungs for a variety of test particles under different experimental conditions. Schlesinger (8) summarized those studies performed in healthy subjects using monodisperse, charge-neutralized, nonhygroscopic, and nonfibrous aerosols. Corrections for different ventilation conditions were not applied. The data as a function of particle size and the breathing mode are given in Figure 7. For mouth and nose breathing, total deposition in humans exhibits a minimum of about 15% for particles in the 0.1- to 1-μm–size range, for which neither impaction nor sedimentation or diffusion are effective in particle displacement. Sedimentation and/or impaction gov-

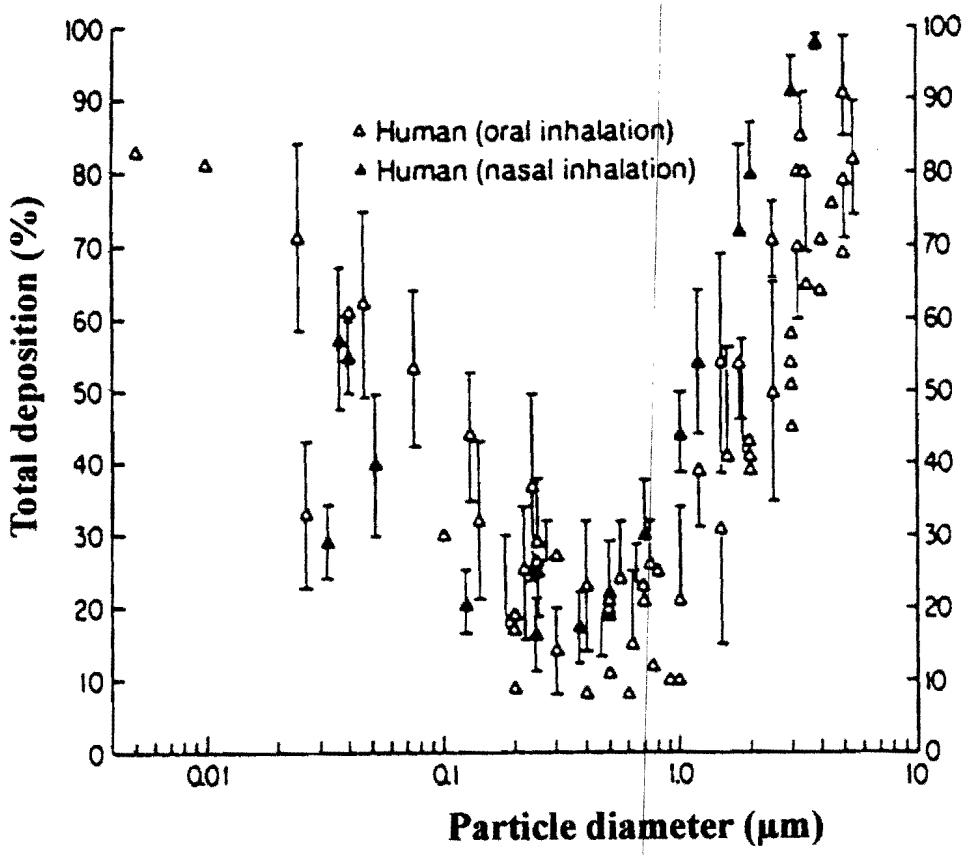

Figure 7 Total deposition data (percentage deposition of amount inhaled) in humans as a function of particle size: Shown are mean values with standard deviations when available. Particle diameters are aerodynamic for those > 0.5 μm and thermodynamic for those < 0.5 μm. (From Ref. 8.)

erns deposition for particles with aerodynamic diameters larger than 1 μm, whereas diffusional displacement determines the deposition of ultrafine particles.

For particles with aerodynamic diameters larger than 1 μm, nasal inhalation generally results in higher total deposition rates than during oral breathing, underlining the greater particle-collecting efficiency of the nasal passage. There is no difference in total deposition between nasal and oral breathing for particles smaller than 1 μm, although little differences for particles in the nanometer range have been reported (169,170).

There is a considerable scatter in the deposition data, although, in general, the same trend can be inferred from the different studies. The heterogeneity may be partly related to the different kinds of test particles and methods applied. But the scatter, in particular, is caused by the intersubject variability in airway morphology and the various breathing patterns used for particle inhalation (71,72,

169–175). Quantifying the biological variability in deposition by the coefficient of variation reveals that, in healthy human subjects, coefficients of 0.38 and 0.19 were observed for 1 and 3-μm–particle deposition under spontaneous-breathing conditions. Under these conditions, coefficients of variation for minute ventilation, tidal volume, and breathing frequency were found to be about 0.2 (176,177). For controlled-breathing conditions, total deposition variability was diminished, and the respective coefficients of variation reduced to 0.27 and 0.13 (71).

Empirical model calculations of total deposition in the human respiratory system are given by Heyder et al. (163) and Rudolf et al. (165–168). From the empirical Eq.(8) for extrathoracic (DE_{ET}), tracheobronchiolar (DE_{TB}), and alveolar deposition (DE_A), total deposition (DE_{Tot}) can be assessed by

$$DE_{Tot} = DE_{ET} + DE_{TB} + DE_A \tag{8}$$

VI. Regional Deposition

A. Extrathoracic Deposition

Even during quiet breathing, flow velocities in the extrathoracic airways are relatively high. Therefore, residence time of particles within these regions is short and most of the airflow through nasal or oropharyngeal airways is turbulent (178,179). For particles in the aerodynamic domain, deposition is governed mainly by impaction. Particle deposition in the ultrafine-sized range is controlled principally by diffusion, but may be enhanced by the complex interactions of diffusion and turbulent airflow (180–182).

Nose Breathing

The specific anatomical features of the nose, such as nasal hairs or the nasal valves, support the high filtration efficiency of the nose and favor deposition mainly at the entrance of the nasal cavity (183). With nose breathing, laryngeal deposition has been neglected by most authors, for most of those particles that are likely to be retained at the larynx have already been removed by the nasal filter. Hence, because deposition only within the nasopharyngeal airways has been considered, extrathoracic deposition during nose breathing has been previously termed nasopharyngeal deposition.

Aerodynamic Domain

Figure 8 summarizes experimental data (184) obtained on inspiratory collection efficiencies of the human nose as a function of the impaction parameter $d_{ae}^2\,Q$ (d_{ae}, aerodynamic particle diameter; Q, respiratory flow rate). This parameter is applied to account for different flow rates and particle sizes between experimental studies. Despite substantial scatter of the data, the particle collection efficiency

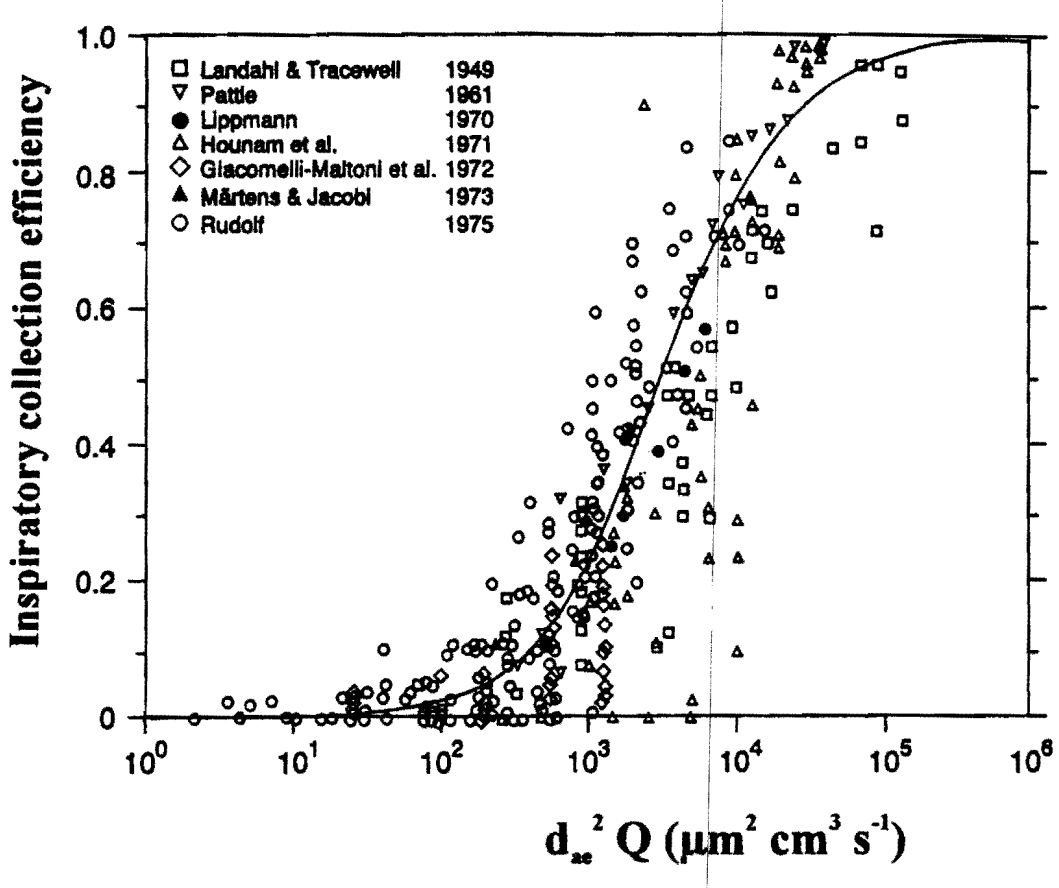

Figure 8 Inspiratory collection efficiency of the human nose as a function of the impaction parameter $d_{ae}^2 Q$: The curve represents a hyperbolic approximation; d_{ae}, aerodynamic particle diameter; Q, inspiratory flow rate. (From Ref. 184.)

of the nose appears to increase in a sigmoidal manner with increasing values of $d_{ae}^2 Q$. The targeting of particles to the nasal region, therefore, requires an aerosol with coarse particles to be inhaled with large flow velocities. For increasing the deposited fraction, it is more effective to increase particle size than flow rate. Mean inspiratory flow rates at rest and exercise are in the order of 250 cm^3 s^{-1} and 1000 cm^3 s^{-1}, so that the respective impaction parameters for 3-μm particles are 2250 μm^2 cm^3 s^{-1} and 9000 μm^2 cm^3 s^{-1}. The latter value also holds for 6-μm particles during quiet breathing. The corresponding experimental data shows nasal deposition efficiencies of 0.05 to 0.6 for 3-μm particles inhaled during quiet breathing. For 3-μm particles inhaled at 1000 cm^3 s^{-1} or for 6-μm particles inhaled at 250 cm^3 s^{-1}, deposition rates are 0.25 to 0.8. The scatter in experimental data is related to mainly the intersubject variability of the anatomical features of the nose (185–187). Cheng and co-workers (185) characterized nasal geometry of ten subjects using magnetic resonance imaging (MRI) and

acoustic rhinometry. They found that particle deposition onto nasal airway walls increases with increasing nasal surface area and airway complexity, and with decreasing nasal cross-sectional area. Also, a significant variability in deposition arises within individuals from physiologically occurring periodic variations in the nasal resistance and cross-sectional area that distribute airflow from one side to the other by as much as 20–80%.

There are several approaches to characterize nasal deposition by mathematical (120,122) or by empirical models (163,165–168,173,184,188,189). For particles of 1 μm or larger, Rudolf et al. (168) estimated inspiratory particle collection efficiency of the nose ($E_{ET\text{-}N}$) by

$$E_{ET\text{-}N} = 1 - (2.05 \times 10^{-4}\, d_{ae}^2\, Q + 1)^{-1} \tag{9}$$

This empirical model assumes the inspiratory flow rate Q to be constant.

Empirical models neglect expiratory nasal deposition, for it appears to be insignificant relative to inspiratory collection efficiency. Stahlhofen (184) considers the fraction of the tidal volume flowing through the nose during inspiration to be $1 - V_{ET}/V_T$. The fraction of particles deposited in the extrathoracic region during nasal breathing $DE_{ET\text{-}N}$ is then given by

$$DE_{ET\text{-}N} = \left[1 - \left(\frac{V_{ET}}{V_T}\right)\right] E_{ET\text{-}N} \tag{10}$$

where V_T is the tidal volume and V_{ET} is the extrathoracic volume. V_{ET} is approximated to 50 cm^3 for male adults and to 40 cm^3 for female adults (168). Deposition data predicted by the model for a tidal volume of 1000 cm^3, at flow rates of 250 $cm^3\ s^{-1}$ and 1000 $cm^3\ s^{-1}$ are shown in Figure 9. For all particles in the aerodynamic size range, the higher flow rate clearly enhances nasal collection efficiency. For a given particle size and flow rate, variations in tidal volume have almost no effect on the fraction of deposited particles [see Eqs. (9) and (10)], but the absolute number or mass of particles retained in the nose changes proportionally with the tidal volume.

Thermodynamic Domain

Deposition of particles of the thermodynamic size range has not been studied extensively in humans. Cheng and co-workers (185) measured deposition efficiencies for 4-, 8-, 20-, and 150-nm particles in ten healthy adult, male volunteers. For nose-in mouth-out breathing at flow rates of 333 $cm^3\ s^{-1}$, deposition fractions for these particle sizes were 36.7 ± 10.6 (mean ± SD), 21.2 ± 8.9, 11.1 ± 7.7, and 5.2 ± 3.8%. However, because expiratory deposition in the mouth is not negligible for particles in the thermodynamic domain, these values overestimate nasal deposition. The large SD values indicate that intersubject deposition variability is notable in the thermodynamic domain. Mean nasal deposition, as de-

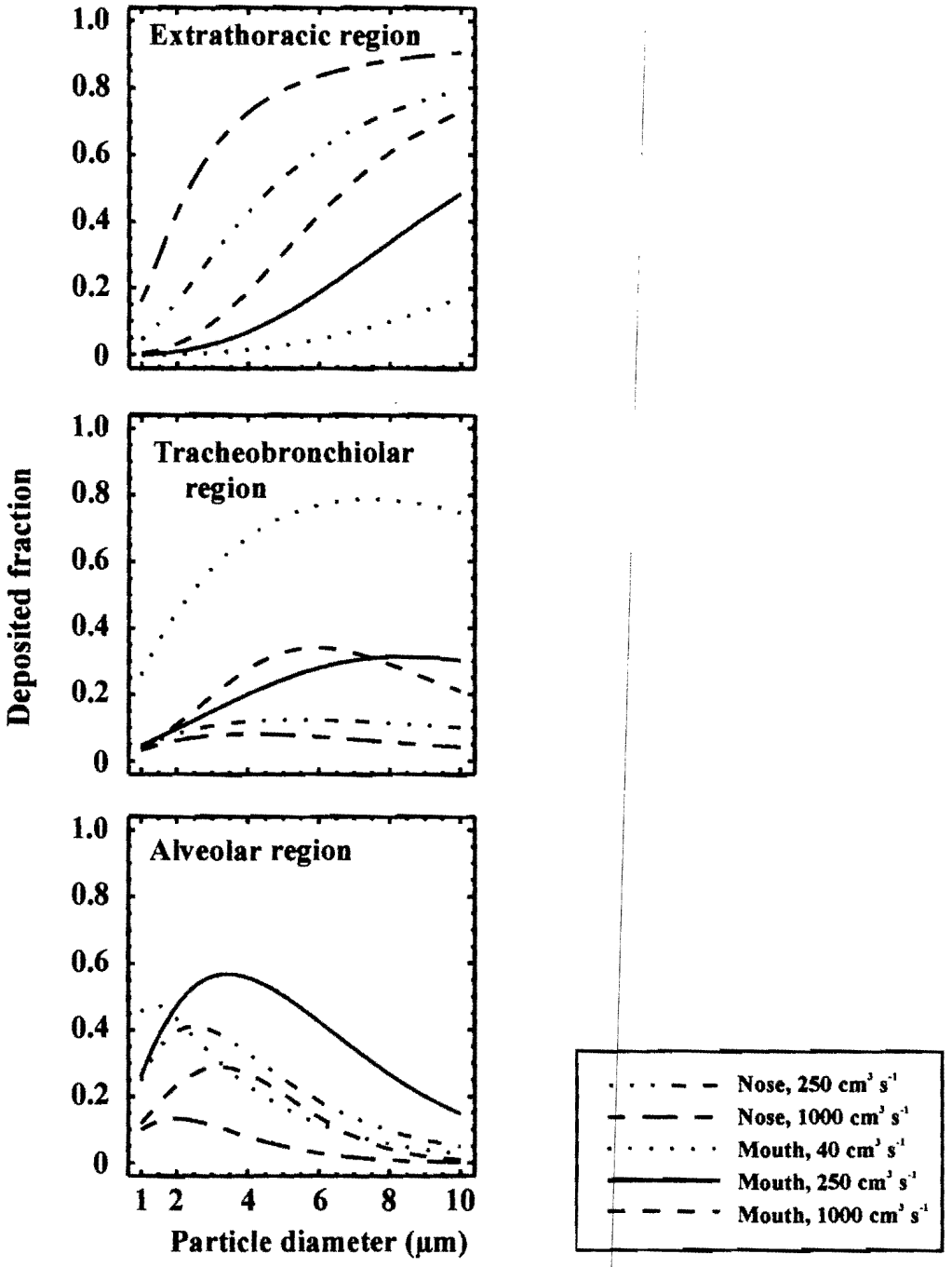

Figure 9 Effect of flow rate on regional deposition: Regional deposition fraction curves are shown for nose and mouth breathing as predicted by the empirical model of Rudolf et al. (167) for male adults. Calculations were performed for a tidal volume of 1000 cm^3 at flow rates of 40, 250, and 1000 $cm^3\ s^{-1}$.

rived from data on total deposition, was estimated to be 15 and 4% for 5- and 10-nm particles at flow rates of 250 $cm^3\ s^{-1}$ (169,170). In the subnanometer-sized range, particle filtration of the nose appears to be almost complete. Inspiratory nasal deposition of 0.53- to 0.62-nm particles ranged between 0.94 and 0.99 in three subjects during quiet-breathing conditions (182).

Complementary to the experiments in human subjects, measurements were performed in hollow replicates of human nasal airway casts (106,108,112,116, 181,190). Particle collection efficiency obtained in nasal airway casts can be approximated by an exponential function of the diffusion parameter (D_p/Q)

$$E_{ET\text{-}N} = 1 - \exp(-12.65\ D_p^{1/2}\ Q^{-1/8}) \tag{11}$$

(112), which indicates that the dependence on respiratory flow rate Q is weaker than that on particle diffusivity D_p. In the thermodynamic domain, expiratory particle collection efficiency of the nose is approximately 10% higher than inspiratory efficiency (106).

Mouth Breathing

Aerodynamic Domain

Figure 10 summarizes human experimental data (184) on extrathoracic deposition during mouth breathing as a function of the impaction parameter $d_{ae}^2\ Q$. There is substantial scatter in the data, but similar to nasal deposition, the dependence on $d_{ae}^2\ Q$ appears to be sigmoidal. However, it must be emphasized that for $d_{ae}^2\ Q < 10^4$, deposition during mouth breathing is considerably smaller than during nose breathing. During a quiet inspiration, the nose retains about 30% of 3-μm particles, whereas less than 5% of the particles are caught in the extrathoracic region with mouth breathing (see also Fig. 9).

Most of the experimental data of Figure 10 were obtained in human subjects inspiring particles through a tubular mouthpiece held between the teeth. Several studies show that this mode of inhalation causes deposition to occur mainly in the larynx, especially on the upper surface of the vocal cords (48,165,191), whereas almost no particles are lost in the oral cavity or the pharynx. Therefore, extrathoracic deposition during mouth breathing was previously termed laryngeal deposition. During natural mouth breathing, deposition in the oral cavity was higher and quite variable depending much on the degree of mouth opening, flow rate, and breathing frequency (172,192,193).

Empirical models (163,165–168,184) characterize oral collection efficiency ($E_{ET\text{-}M}$) for particles 1 μm or larger, as a function of the impaction parameter $d_{ae}^2\ Q$:

$$E_{ET\text{-}M} = 1 - [1.1 \times 10^{-4}\ (d_{ae}^2 \times Q^{0.6} \times V_T^{-0.2})^{1.4} + 1]^{-1} \tag{12}$$

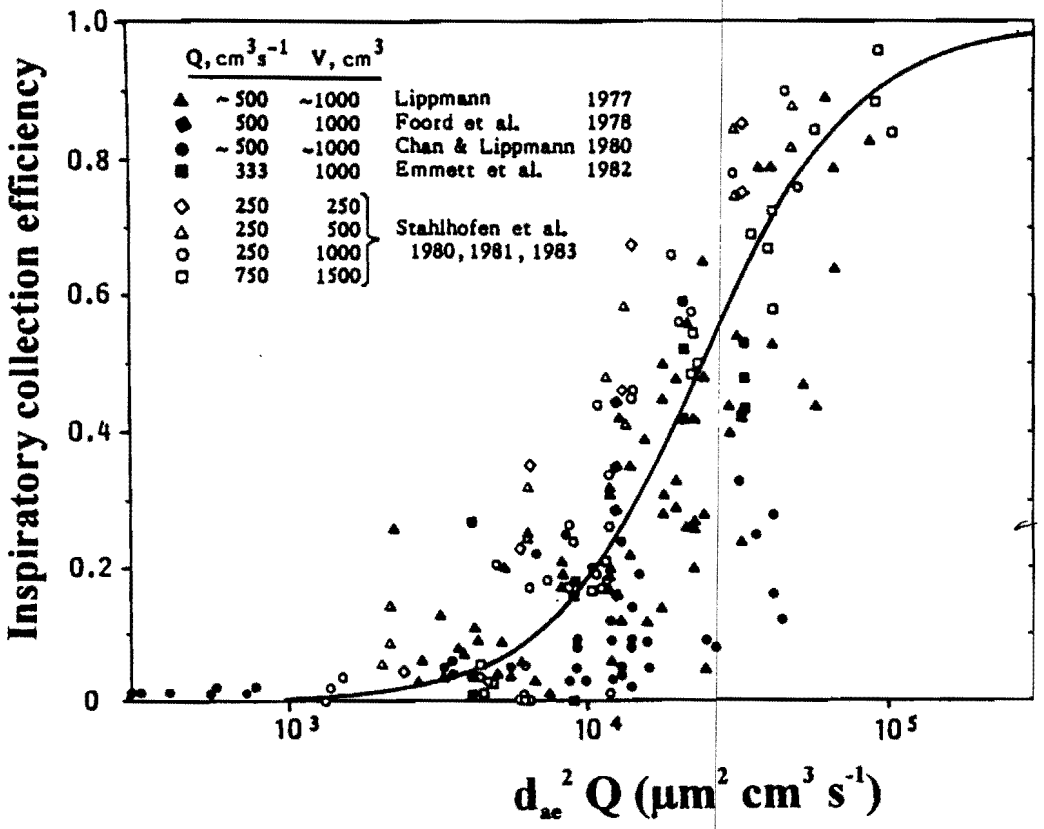

Figure 10 Inspiratory extrathoracic deposition data in humans during mouth breathing as a function of the impaction parameter d_{ae}^2 Q: The curve represents a hyperbolic approximation. d_{ae}, aerodynamic particle diameter; Q, inspiratory flow rate. (From Ref. 184.)

Extrathoracic deposition during mouth breathing ($DE_{ET\text{-}M}$) is derived from the collection efficiency weighted by the fraction of tidal volume ($1 - V_{ET}/V_T$) flowing through this region

$$DE_{ET\text{-}M} = \left[1 - \left(\frac{V_{ET}}{V_T}\right)\right] E_{ET\text{-}M} \tag{13}$$

Expiratory deposition is again considered to be negligible in comparison with inspiratory deposition (163,184). Figure 9 shows deposition data predicted by the model for breathing conditions during rest and exercise. The model assumes a constant respiratory flow rate Q, but takes into account that the collection efficiency decreases with increasing tidal volume V_T. It shows that oral deposition is less dependent on flow rate than is nasal deposition, as Q is weighted by a power exponent of 0.6. Therefore, the aerodynamic particle diameter is the main

determinant of oral collection efficiency and, for targeting particles into this region, coarse particles should be inhaled (see Figs. 9 and 13). Moreover, for increasing the deposited fraction of particles, it is much more efficient to increase particle size than flow rate. Similar to nose breathing, the fraction of particles deposited in the oral region, for a given particle size and flow rate, is generally independent of the tidal volume inhaled [see Eqs. (12), (13); Fig. 11]. But one must consider that the number or the mass of removed particles increases almost linearly with increasing tidal volume.

Thermodynamic Domain

Oral deposition of ultrafine particles determined in physical replicates of oropharyngeal airways was slightly smaller than that measured in nasal casts (109,181,194). However, measurements performed in three healthy adults suggest that there is zero deposition for 0.1-, 0.07-, and 0.05-μm particles inhaled through the mouth under different breathing conditions (163).

B. Intrathoracic Deposition

Experimentally determined deposition efficiencies of the intrathoracic region have usually been inferred from measurements with radioactively labeled particles. The fast-cleared fraction of thoracic activity has been assumed to be deposited in the tracheobronchiolar region, whereas the slow-cleared fraction has been assigned to the alveolar region of the lung (see Chap. 7). Recently, this distinction has become a matter of controversy, for experiments suggest that some of the activity deposited in the conducting airways is cleared much slower than previously assumed (30–32). Some investigators, therefore, prefer to use the term "fast-cleared and slow-cleared thoracic deposition," instead of tracheobronchiolar and alveolar deposition, for the description and analysis of deposition studies using radioactivity.

Tracheobronchiolar Deposition: Fast-Cleared Thoracic Deposition

Aerodynamic Domain

Particles escaping from deposition in the extrathoracic regions enter the lung through the tracheobronchiolar airways. Because flow velocities in the airways decrease rapidly from large to small conducting airways, inertial impaction determines particle deposition only in the most central airways. With decreasing airway diameter, gravitational sedimentation gains more and more importance and dominates deposition within the small bronchial airways. As inertial impaction grows stronger with increasing particle mass, the site of deposition is shifted from the peripheral to the proximal airways with increasing particle size (see Figs. 14 and 15). During expiration, only sedimentation is of importance, because those larger particles that escape inertial deposition during inspiration are subse-

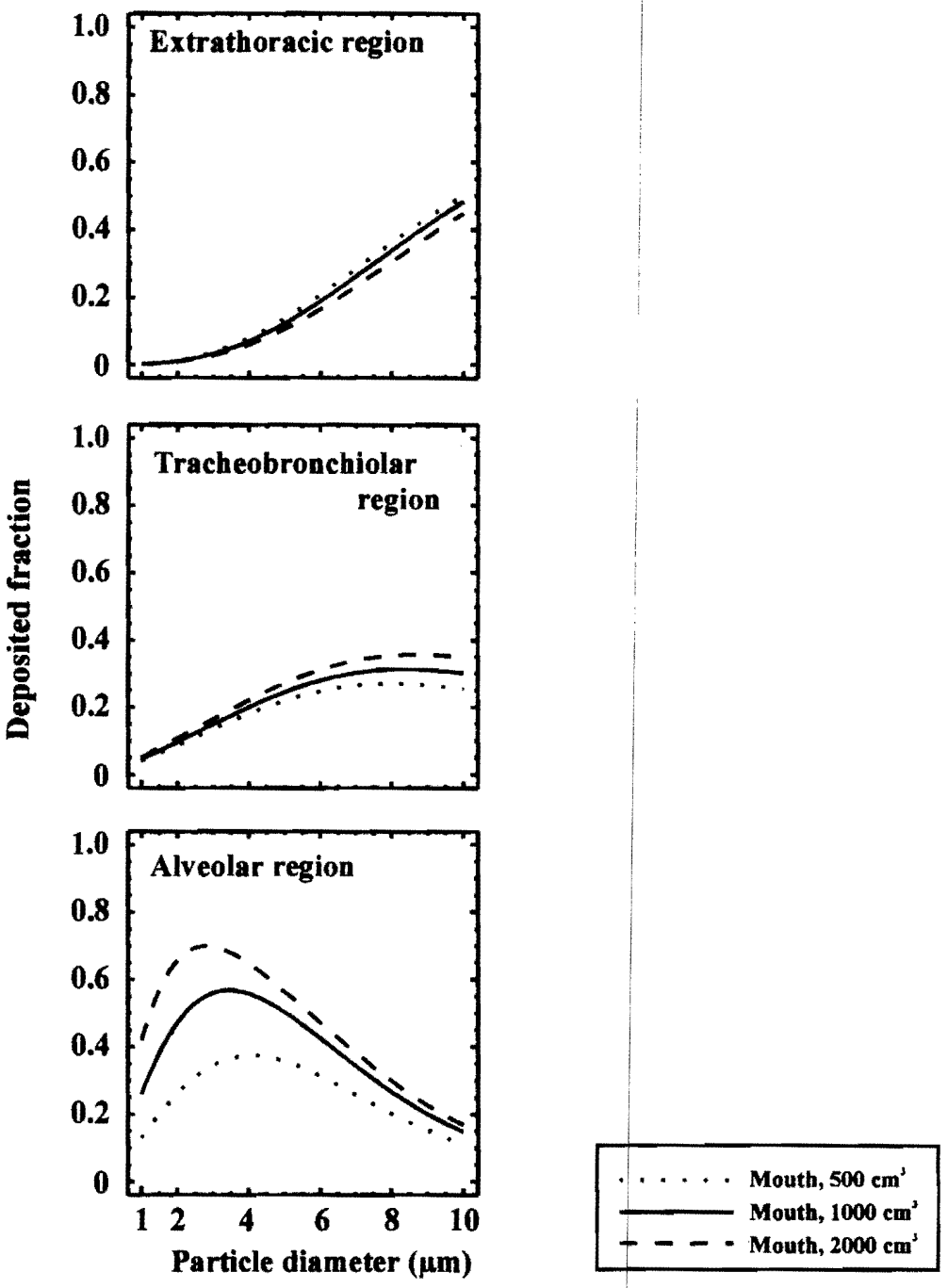

Figure 11 Effect of tidal volume on regional deposition: Regional deposition fraction curves are shown for mouth breathing as predicted by the empirical model of Rudolf et al. (167) for male adults. Estimates were done for tidal volumes of 500, 1000, and 2000 cm^3 at a flow rate of 250 $cm^3\ s^{-1}$.

quently collected in the small conducting airways or in the alveolar region of the lung.

Experimental data, from several investigators who measured intrathoracic particle deposition during mouth breathing, were summarized by Stahlhofen et al. (184). Figure 12 shows these data as a function of the aerodynamic particle diameter. Because large particles are effectively collected by the extrathoracic airways, intrathoracic deposition does not increase or decrease monotonically with particle diameter, but exhibits maximal values for particles with diameters between 4 and 8 μm. It appears to be lowest for particles smaller than 1 μm.

There is a remarkable variability between deposition data collected in different studies. As an example, deposition of 3-μm particles may range between almost zero and a particle loss of close to 50%. Beside those subject-specific factors cited before, technical and experimental confounders are discussed. There were significant differences in measuring procedures and in definitions applied to describe the fast-cleared portion of thoracic particles (184). Moreover, recent investigations suggest hygroscopic growth and leaching of test particles as a possible source of measurement error, resulting in an overestimation of the deposited fraction.

Empirical models (163,165–168) characterize the collection efficiency of the tracheobronchiolar region (E_{TB}) for particles 1 μm or larger as:

$$E_{TB} = 1 - \exp\{-1.24\,[4 \times 10^{-6}\,CF^{2.8}\,(d_{ae}^2\,Q)^{1.15}] - 1.24\,[(0.009 + 0.165\,t_b^{1.5})\,d_{ae}\,t_b^{-0.25}]\} \quad (14)$$

CF is a correction factor accounting for gender. It is 1 for adult men and 1.075 for adult women. The residence time of particles in small bronchial airways, t_b, is

$$t_b = \frac{V_{b\text{-}FRC}\,(2 + V_T/FRC)}{2\,Q} \quad (15)$$

V_T is the tidal volume and FRC is the functional residual capacity of the lung. FRC is assumed to be 3300 cm^3 for male and 2660 cm^3 for female adults in the coefficients for Eq. (14). $V_{b\text{-}FRC}$ represents the volume of the small bronchial airways at an FRC level, set to 48 and 39 cm^3 in adult men or women (168). Equation (14) characterizes inertial E_{TB} relative to the impaction parameter $d_{ae}^2\,Q$, and sedi-

Figure 12 Tracheobronchial and alveolar deposition data in humans during mouth breathing as a function of aerodynamic particle diameter: The solid curves represent the approximate mean of all experiments, the broken curve gives a "conservative" estimate based on data by Stahlhofen et al. (From Ref. 184.)

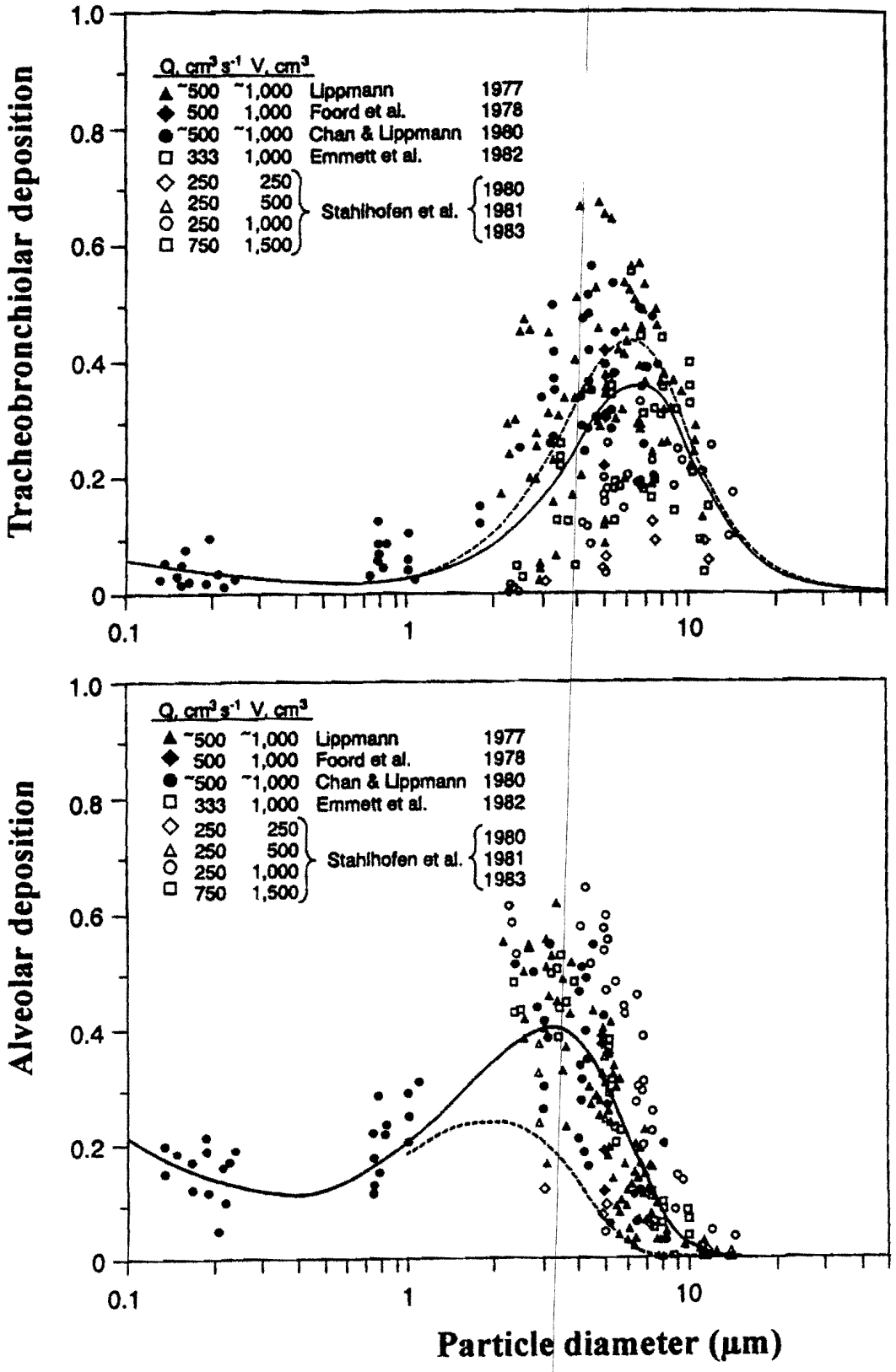
Tracheobronchiolar deposition
Alveolar deposition
Particle diameter (μm)
Q, cm³ s⁻¹ V, cm³
~500 ~1,000 Lippmann 1977
500 1,000 Foord et al. 1978
~500 ~1,000 Chan & Lippmann 1980
333 1,000 Emmett et al. 1982
250 250
250 500
250 1,000
750 1,500
Stahlhofen et al. 1980 1981 1983
0
0.2
0.4
0.6
0.8
1.0
0.1
1
10

mentational E_{TB} by considering particle diameter and the residence time of particles in small bronchial airways. It further accounts for the expansion of airways during inhalation, but it is based on a constant respiratory flow.

Because the number of particles deposited in the tracheobronchiolar region will be decreased by particle losses during inspiration in the extrathoracic region $(1 - E_{ET})$, the empirical expression for tracheobronchiolar particle deposition (DE_{TB}) is

$$DE_{TB} = \left[1 - \left(\frac{V_{ET}}{V_T}\right)\right](1 - E_{ET})\,E_{TB} \tag{16}$$

Depending on the mode of breathing, E_{ET} is the deposition efficiency for mouth breathing $(E_{ET\text{-}M})$ or for nose breathing $(E_{ET\text{-}N})$.

Targeting Particles into the Tracheobronchiolar Region

The deposited fractions of particles, as predicted by the foregoing model, are presented in Figures 9 and 11. For targeting particles into the tracheobronchiolar region, the mode of choice is obviously mouth breathing (see Fig. 9). Within the physiological range of flow velocities, inhaling at 1000 $cm^3\ s^{-1}$ leads to somewhat higher deposition of particles between 3 and 7 μm, with a slight peak at 6 μm. However, this high flow rate also causes extrathoracic deposition to double (see Fig. 9), which because of possible side effects often must be avoided in inhalation therapy. In this situation, inhaling particles between 4 and 6 μm at 250-$cm^3\ s^{-1}$ inspiratory flow appears to be appropriate for targeting particles to the tracheobronchiolar region and for keeping extrathoracic deposition low.

However, in inhalation therapy, the mass of the therapeutic substance delivered to the extrathoracic, tracheobronchiolar, or alveolar region by the deposited particles is the primary parameter of interest. This mass, in fact, depends on the deposited fraction, but it is essentially determined by the output of the nebulizer. The output of a nebulizer, in return, depends on the nebulized number of particles per volume element and the produced particle size. The size is of importance because the mass of a particle increases substantially with increasing particle diameter (see Table 1). To illustrate this, based on the deposition fractions given in Figure 9, the amount of substance delivered to the three regions by 1000 inhaled unit-density spheres during mouth breathing was determined for particle sizes between 0.1 and 10 μm. The results in Figure 13 show that the total mass

Figure 13 Amount of substance deposited per 1000 inhaled unit-density spheres in the extrathoracic, the tracheobronchial, and the alveolar region during mouth breathing for a tidal volume of 1000 cm^3 and flow rates of 40, 250, and 1000 $cm^3\ s^{-1}$. Estimates are based on deposition fractions given in Figure 9.

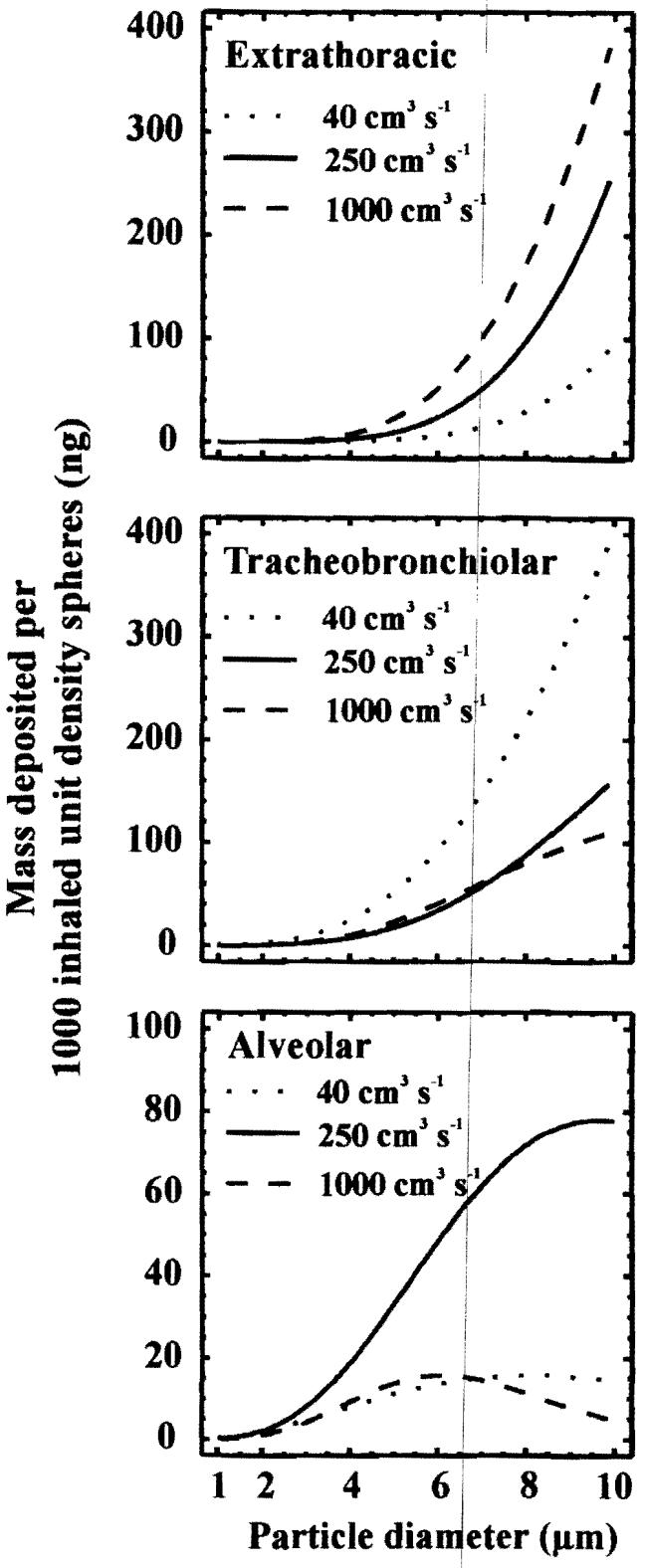
Extrathoracic
40 cm³ s⁻¹
250 cm³ s⁻¹
1000 cm³ s⁻¹
Tracheobronchiolar
Alveolar
Mass deposited per 1000 inhaled unit density spheres (ng)
Particle diameter (μm)
0
100
200
300
400
20
40
60
80
1
2
4
6
8
10

deposited in the extrathoracic region during mouth breathing increases considerably for particles larger than 4–6 μm during quiet breathing, but even more during exercise. The amount of therapeutic substance deposited in the tracheobronchiolar region is comparable for any particles smaller than 8 μm at 250 or at 1000 cm^3 s^{-1}. For larger particles, despite a decrease in the deposited fraction (see Fig. 9), the mass delivered to the tracheobronchiolar region still increases, slightly more at 250 cm^3 s^{-1} than at 1000 cm^3 s^{-1}. Therefore, the breathing mode of choice is quiet inhalation of 4- to 6-μm particles if extrathoracic deposition must be avoided. If extrathoracic deposition is noncritical, about five times more therapeutic substance can be deposited per breath in the tracheobronchiolar region when 8- to 10-μm particles are inhaled with quiet mouth breathing. These estimates, however, do not take into account that, with "real" nebulizers, the number output usually decreases with increasing particle size. But according to Ferron et al. (195), this is less than a factor of 5 for the particle size range of interest.

The deposited fraction in the conducting airways is almost independent of tidal volume (see Fig. 11), so that the total number of deposited particles changes in proportion to the inhaled aerosol volume. Augmentation of the inhaled volume by an increase in tidal volume also increases alveolar deposition (see Fig. 11 and next paragraph), such that if a low alveolar deposition is required, inhalation of repeated small tidal volumes appears to be more appropriate than that of fewer but larger ones.

Recently, an interesting new approach to target 6-μm particles into the conducting airways was proposed by Anderson (196) and Svartengren (197). They used very slow inspiratory flow rates, of about 40 cm^3 s^{-1}. At this flow rate, the residence time within the conducting airways is long, and deposition is entirely related to sedimentation, which causes the retained fraction in the tracheobronchiolar region to increase substantially. Predicted deposition rates for this type of breathing maneuver are included in Figure 9. The deposited fraction can be expected to be almost constant and larger than 0.6 for particles larger than 4 μm. Owing to the diminished effects of impaction, extrathoracic deposition in the larynx is substantially decreased in comparison with the physiological flow rates discussed in the foregoing (see Fig. 9). Extrathoracic deposition is less than 0.05 for particles smaller than 6 μm and close to 0.1 for 8-μm particles. The corresponding amount of material deposited in the larynx or in the conducting airways can be inferred from Figure 13. If we consider all effects, 6- to 8-μm particles appear to be most suitable for very slow inhalation procedures. The notably enhanced amount of substance delivered to the tracheobronchiolar region makes this technique a very interesting approach for new inhalation therapies. However, specific devices have to be applied for patients to be able to maintain such low flow rates.

Thermodynamic Domain

Experiments performed in three healthy adults who inhaled 0.1-, 0.07-, and 0.05-μm particles, using various breathing maneuvers, showed that these particles are not retained in the tracheobronchiolar airways (163).

Alveolar Deposition: Slow-Cleared Thoracic Deposition

Aerodynamic Domain

Those particles escaping the extrathoracic and the tracheobronchiolar filters reach the alveolated region of the lung. Figure 12 summarizes alveolar deposition during mouth breathing (184), data are taken from the same studies as the foregoing. Discrepancies between studies appear to be less pronounced than for tracheobronchiolar deposition. Alveolar deposition probability peaks at about the same particle size range as does tracheobronchiolar deposition, but a slight advantage for smaller particles to be deposited in the alveoli is detectable. Deposition for particles smaller than 1 μm is twice as likely in the alveoli as in the conducting airways.

The dominant mechanism resulting in alveolar particle deposition is gravitational settling, in addition diffusional displacement becomes more and more significant for particles smaller than 0.5 μm (see Table 1). The efficiency of the alveolar region to collect particles owing to their sedimentation is determined by considering the distance a particle settles while staying in this region. Accordingly, in empirical expressions (163,165–168) the deposition efficiency in the alveolar region (E_A) is assessed as a function of the parameter $d_{ae}^2\, t_A$ for particles 1 μm or larger.

$$E_A = 1 - \exp\left[-0.171\ \mathrm{CF}\ (d_{ae}^2\, t_A)^{2/3}\right] \tag{17}$$

where t_A is the residence time of particles during inspiration in the alveolar region:

$$t_A = \frac{V_T - V_D}{Q} \tag{18}$$

CF is a correction factor applied for gender, V_D is the dead space volume, composed of the extrathoracic and the tracheobronchiolar volumes. It is approximated to 147 and 118 cm^3 for male and female adults (168). The deposited fraction in the alveolar region (DE_A) is

$$DE_A = \left[1 - \left(\frac{V_D}{V_T}\right)\right](1 - E_{ET})\,(1 - E_{TB})\,E_A \tag{19}$$

where E_{ET} is the deposition efficiency for mouth breathing ($E_{ET\text{-}M}$) or for nose breathing ($E_{ET\text{-}N}$).

Targeting Particles into the Alveolar Region

Differences in DE_A between nose and mouth breathing, as predicted by the empirical model, are shown in Figure 9. For each flow rate, differences in alveolar deposition become obvious for particles larger than 1.5 μm, because large particles undergo effective filtration in the nose. Because the collection efficiency of the upper airways is small for small particles, most of the inspired particles smaller than 1.5 μm reach the alveolar region. Given the model data presented in Figure 9, the mode of choice for an inhalation therapy aimed at targeting particles into the alveolar region is quiet inhalation of an aerosol with 2- to 4-μm particles during mouth breathing. This provides about 50% of the inhaled particles to this region and keeps the burden delivered to the extra- and intrathoracic airways low (see Figs. 9 and 13). Increasing tidal volume while maintaining a low flow rate further increases alveolar deposition (see Fig. 11) because particles are convectively transported deeper into the lung and the residence time of particles in the alveolar region is increased. Similarly, a breath-hold, performed at end-inspiration, improves the collection efficiency. According to the empirical model, for instance, a 1000-cm^3 breath, inhaled at 250 $cm^3\ s^{-1}$, results in 55% deposition of 3-μm particles in the alveolar region. A 3-s breath-hold at the end of inspiration enhances deposition to 65%.

Thermodynamic Domain

There are almost no experimental data on alveolar deposition available for this domain. Heyder et al. (163) measured deposition in three healthy adults for 0.1-, 0.07-, and 0.05-μm particles. At a flow rate of 250 $cm^3\ s^{-1}$ and a tidal volume of 500 cm^3, alveolar deposition was 21, 27, and 33%. Increasing tidal volume to 1000 cm^3, while keeping the flow rate constant, raised the removed fraction consistently to values of 34, 43, and 52%. With a flow rate of 750 $cm^3\ s^{-1}$ and a tidal volume of 1500 cm^3, deposition was 25, 36, and 45%. Independent of the breathing maneuver, the fraction of particles collected in the alveolar region increased with decreasing particle size. Both the residence time and the tidal volume appear to be significant determinants of particle deposition in this region.

VII. Factors Modifying Particle Deposition

A. Lung Geometry: Age- and Gender-Specific Differences

During development from infancy to adulthood, the respiratory system undergoes substantial changes in airway structure and lung volume, accompanied by considerable differences in spontaneous-breathing conditions (198–206). Even in adults, distinct sex-related and racial differences are established for structural and conventional lung function parameters (207–211). However, only limited

information is available in how far particle deposition in the respiratory system is affected by age, gender, or race.

Deposition in Infants and Children. For this population, deposition data are rare (212–215). Total deposition of particles sized 1–3 μm was measured in 29 healthy children (6.7–14 years) during controlled and spontaneous mouth breathing (214,215), using the respiratory aerosol probe (see Sec. IV.A, under Noninvasive Techniques). Spontaneously breathing children exhibited slightly smaller tidal volumes than adults, but had a higher respiratory rate, so that minute ventilations were almost identical. As in adults, total deposition in children increased with increasing particle size, being approximately 15% for 1-μm particles, 50% for 2.3-μm particles, and 75% for 3-μm particles. The intersubject variability observed in children was comparable with that in adults. For spontaneous, as well as for controlled breathing, deposition decreased slightly with increasing body size, suggesting that smaller lung dimensions favor deposition. This assumption is supported by the fact that deposition values for all particle sizes are higher in children than in adults. In comparison with adults, total deposition in children was increased by an average factor of 1.5, ranging between 1.2 and 1.9 for different particle sizes and breathing patterns. Furthermore, the amount of particles deposited per unit surface area is increased by a factor of 4–5 in children, because the surface area of their respiratory system is only about one third (40 m^2) that of adults (5).

We are unaware of deposition studies in healthy neonates or infants, probably owing to concerns over the use of radiotracers in this population (33). There are some deposition studies, related to therapeutic drug delivery, in spontaneously breathing or ventilated infants with lung diseases (216–218). Also, filter and animal lung models have been used to assess deposition in infants (219–222). One of the limitations of these studies is that deposition is often related to the amount of radioactivity delivered into the nebulizer unit and not to what is actually inhaled. Hence, there is a clear necessity for improved deposition studies to better understand health risks from environmental air pollutions or to improve inhalation therapy in neonates and infants.

Gender Differences in Adults

Lung structure and breathing pattern are considered to be different in adult men and women. The average female thorax is smaller, and the conducting airway size is only about 75% that in men (223). In addition, resting minute ventilation and respiratory flow rates are lower in women than in men. During controlled as well as spontaneous mouth breathing, deposition of particles of the aerodynamic domain was slightly, but consistently, lower in women than in men (213,224,225). Analysis of regional deposition revealed that this was related to a higher extrathoracic and tracheobronchiolar deposition rate (225). Considering that deposition within these regions is largely determined by impaction, deposi-

tion was reassessed as a function of the impaction parameter d_{ae}^2 Q. Still there remained an unexplained few percent difference between deposition in women and in men. This difference was most likely attributed to structural differences between men and women (225) in the conducting airways. The empirical model calculations introduced earlier try to account for that by applying a correction factor and by considering gender-specific lung and airway volumes.

B. Exercise

Adults. Ventilation is increased during exercise according to the higher oxygen demand of the body. In adults, this is usually accomplished by an increase in tidal volume and breathing frequency; hence, respiratory flow rates are also high. In addition, breathing is often switched from the nasal to an oronasal or oral route, especially at high levels of exercise (193). In some studies (213,225), total deposition estimated breath-by-breath increased for 1- to 5-μm particles in male and female adults, even during light exercise. Other studies failed to detect clear changes in the deposition rate per breath under various levels of exercise (226,227). Deposition studies under controlled-breathing conditions (70,170) show that increasing tidal volume at a given respiratory rate increases total deposition for all respirable particles. These changes are minimal for particles between 0.1 and 1 μm, for which total deposition is small. Keeping tidal volume constant while increasing respiratory rate decreases total particle deposition for all particle sizes. The most obvious changes here are in the transitional particle-size range. Hence, because of individual breathing patterns, individual features of lung geometry, and different particle sizes studied, physical exercise may result either in an unchanged or an enhanced deposition rate per breath. This is also reflected by a remarkably increased intersubject variability in particle deposition during exercise. Despite these individual differences, the increase in minute ventilation from rest to exercise always enhances deposition per unit of time. This increase is roughly proportional to the increase in minute ventilation.

Children. For particle sizes between 1 and 3 μm, deposition under ventilatory conditions of rest and light exercise was measured in 41 children by Becquemin et al. (212,213). Exercise caused per-breath deposition of 1-μm particles to decrease from about 20 to 15%, whereas the deposition of 2- and 3-μm particles was almost unaffected. Because the higher ventilatory demand under light exercise was accomplished mainly by an increase in breathing frequency, respiratory flows were increased, but the residence time of particles in the respiratory system was shortened. This caused 1-μm particle deposition, which is mainly governed by sedimentation, to decrease. It appears that, for 2- and 3-μm particles, the decreased deposition probability by sedimentation was balanced by an increased effect of impaction, so that total deposition remained unaffected. Therefore, it may be speculated that regional deposition was affected with a partial shift in

deposition toward more central airways. Again, it is important to emphasize that the increase in minute ventilation in response to exercise increased deposition per unit of time considerably for all three particle sizes despite a decreased or unchanged deposition rate per breath.

C. Influence of Gas Composition

Replacing ambient air nitrogen (N_2) by carrier gases with differing physical properties is expected to alter flow profiles in the conducting airways, thereby affecting convective particle transport and deposition patterns within the lungs. According to basic fluid dynamics, alteration of kinematic viscosity (η/σ) is presumed to result in more laminar flows in the airways when N_2 is replaced by helium. More turbulent flow occurs when sulfurhexafluoride (SF_6) is used as a carrier gas, which has about five times the molecular weight of N_2 (228).

Svartengren (229) and Anderson and co-workers (230,231) studied 2.5-μm–Teflon particle deposition (ρ, 2.13 kg m^{-3}; d_{ae}, 3.6 μm) in healthy subjects with and without induced bronchoconstriction and in patients with asthma breathing air or a helium–oxygen mixture (He–O_2). More laminar airflow owing to the use of He–O_2 shifted the site of particle deposition to the lung periphery and resulted in higher deposition rates in the alveolar region, but in lower rates in mouth, throat, and in the tracheobronchiolar region. This effect was more marked for constricted airways, both in healthy subjects with a two- to threefold increase in airway resistance and in asthmatics. It was more pronounced at higher, than at moderate, flow rates. Schulz et al. (232) applied the series bolus delivery technique (see Sec. IV.A, under Noninvasive Techniques) in mechanically ventilated dogs to study local deposition of smaller particles in different gas compositions. Deposition of 0.5-, 1-, and 2-μm particles, was unaltered breathing He–O_2. In SF_6–O_2, the deposited fraction of 2-μm particles was enhanced throughout the lung. It was increased for 1-μm particles in deep lung regions, but it was generally not affected for 0.5-μm particles.

These results show that the extent and the preferable site of particle deposition within the lungs can be modified by the physical properties of the atmospheric carrier gas. However, specific combinations of particle properties and flow fields within the airways are required.

VIII. Local Particle Deposition

Numerous studies have been carried out in the last decades to obtain detailed information about collection efficiencies and deposition patterns on a subregional level within the respiratory system. A complete overview is beyond the scope of the present chapter, but the studies introduced in the following discussion should give the reader an idea about approaches and results.

A. Local Deposition Within the Tracheobronchiolar and Alveolar Region

Gerrity and co-workers (129) modeled local deposition in the tracheobronchiolar tree. Estimates were based on the morphometric lung model proposed by Weibel (5) and on Landahl's formalism of particle deposition (121; see Sec. IV.B, under Mathematical Models). Deposition in each of the airway generations was assessed at a tidal volume of 700 cm^3, a flow rate of 500 $cm^3\ s^{-1}$, and a breath-hold of 0.5 s at end-inspiration. Figure 14 shows the results given as percentage of deposition per airway generation for particles with aerodynamic diameters ranging between 1.6 and 15.8 μm. The percentage quoted is the deposited fraction of those aerosol particles that pass through the glottis. The smallest particles exhibited expected deposition rates below 2% in the conducting airways (generation number 0–16) and a clear tendency to deposit in more peripheral lung structures. For 3.2- and 4.8-μm particles, deposition followed principally the same pattern, but was enhanced both in the lung periphery and in the conducting airways. Deposition of 4.8-μm particles appeared to peak at airway generations 3–7. For particles larger than that, the deposition pattern changed, in that the deposited fraction was reduced in the lung periphery and the predominant site of particle deposition was shifted toward central airways. Peak deposition occurred at the fifth airway generation, ranging between 7 and 16% for 8- and 15.8-μm particles. Relative to health effects from inhaled particles, the authors calculated the surface area densities of deposited particles in the various airway generations. Peak density occurred at generation 3 (i.e., within the segmental and subsegmental bronchi), and it was orders of magnitude higher there than in smaller conducting airways or in peripheral lung structures. This observation is interesting in light of studies done on the frequency and location of bronchial carcinomas (111,233). There was a close correspondence between deposition density and frequency of reported cancer at those sites.

Recently, Kim and co-workers (67) applied the series bolus delivery technique (see Sec. IV.A, under Noninvasive Techniques) to assess local deposition in the lungs of 11 healthy young adults. During mouth breathing, 1-, 3-, and 5-μm particles were inhaled at flow rates of 150, 250, and 500 $cm^3\ s^{-1}$ and at a tidal volume of 500 cm^3. Local collection efficiencies and deposited fractions were determined for ten volumetric lung compartments (50–500 cm^3). For all particle sizes and flow rates, local collection efficiency increased with increasing volumetric lung depth of the compartment. For the highest flow rate, collection efficiency was lowest throughout all compartments. The deposited fraction of 1-μm particles varied per volumetric lung compartment between almost zero and 3%, with a tendency for higher deposition rates in larger lung depth if lower flow rates were applied (Fig. 15). With increasing particle size, deposition was enhanced, and the preferential site of deposition was shifted from the distal to

the proximal compartments of the lung. Peak deposition occurred in volumetric lung regions between 75 and 200 cm^3; it was approximately 15% for 5-μm particles independent of flow rate. Based on the morphometric lung model of Weibel (5), surface area concentrations were estimated and were greater in the most proximal region of the lung than in distal parts, regardless of particle size and flow rate.

When comparing the experimental data with those modeled by the same group (129), there is reasonable agreement for peak values and general patterns of local deposition within the conducting airways (i.e., within a volumetric lung region of 200 cm^3 or the first 16 airway generations). Absolute estimates of deposition within the tracheobronchiolar region, however, are higher than the corresponding experimental values. For example, Kim and co-workers reported tracheobronchiolar deposition of 3- and 5-μm particles to be 11 and 26% for a flow rate of 250 $cm^3\ s^{-1}$, whereas approximately 30 and 50% are expected from the model (see Fig. 14). This disagreement may be partly explained by the differences in breathing pattern and by other factors already discussed by the authors (67). However, it shows that despite the large body of knowledge gained in the past 50 years, there is still a clear necessity for close cooperation between experimental and theoretical researchers to further improve the understanding of even the most basic processes governing particle deposition in the respiratory tract.

B. Local Deposition Within Airway Bifurcations

Collection efficiencies and deposition patterns of inhaled particles on the level of bifurcating airways have been studied experimentally in idealized y-shaped tube models (98,99). The dimensions of the single bifurcation models were adapted from Weibel's human lung data for airway generations 3–5. Branching patterns of the bifurcation were varied for branching angles, geometric symmetry of daughter tubes, and symmetry of flow division at the bifurcation. To assess local deposition patterns within each of the model tubes, the parent and daughter tubes were divided into several sections. Fluorescent-labeled particles of 3, 5, and 7 μm were applied for laminar and transitional flow and the number of particles deposited in each of the tube sections was inferred from fluorometric measurements. During inhalation, collection efficiency in airway models increased with increasing flow rate and particle size, ranging for 3-μm particles, between almost zero deposition and 15%, and for 7-μm particles, between 20 and 70%. Total deposition appeared to be almost independent of the branching angle of daughter tubes, even for asymmetrical branching models. An even inspiratory airflow division at the bifurcation resulted in balanced deposition rates in the two daughter branches. But even with uneven inspiratory flow divisions of as much as 1:3 between daughter branches, deposition efficiencies and patterns deviated only slightly from that of even flow division. The distribution of deposited material

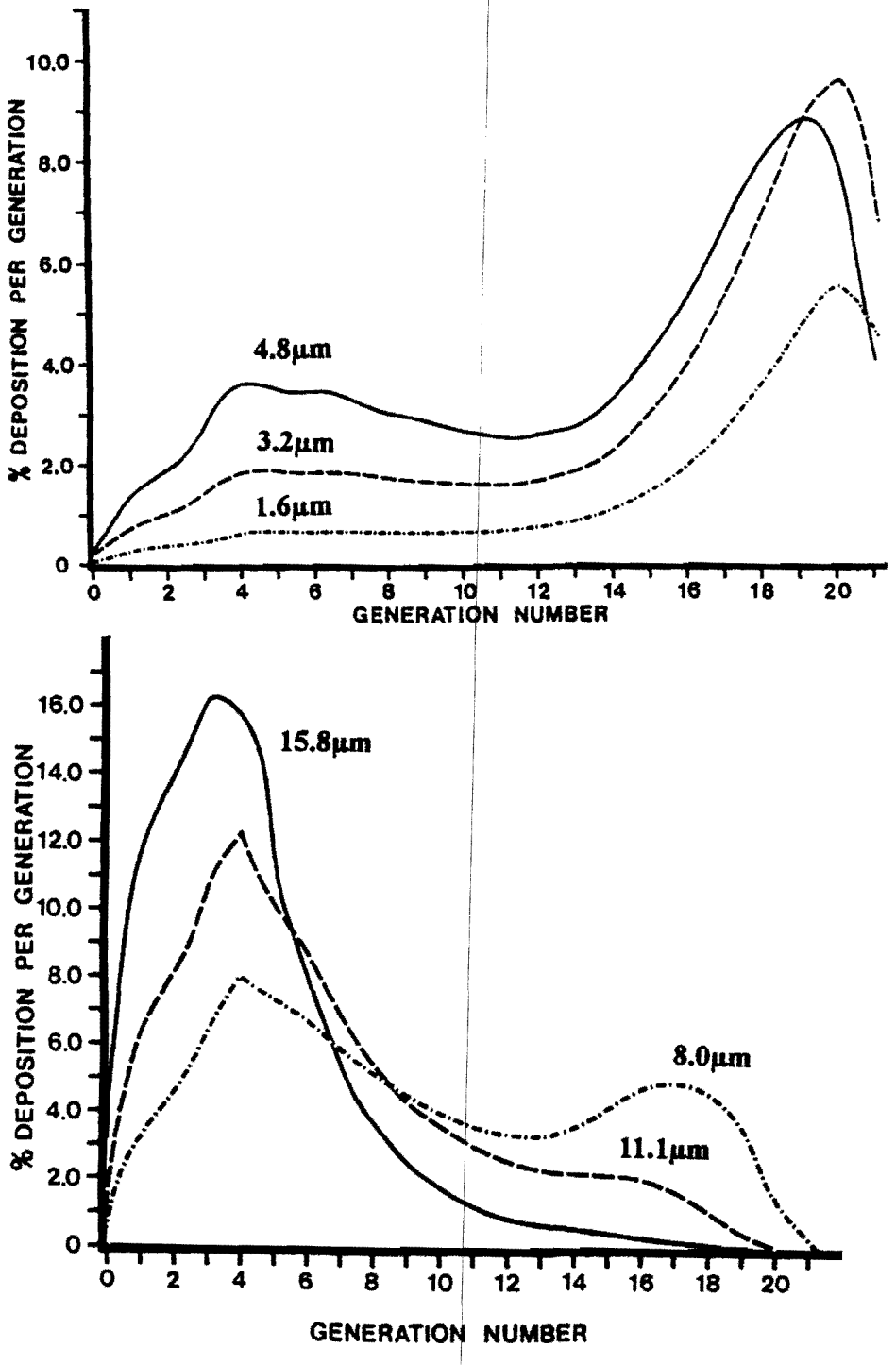

Figure 14 Modeled local deposition in the tracheobronchial and alveolar region: Deposition estimates were carried out for the symmetrical morphometric model of Weibel (5) at a tidal volume of 700 cm^3, an inspiratory flow rate of 500 $cm^3\ s^{-1}$, and an end-inspiratory pause of 0.5 s. The percentage deposition per airway generation is given for particles with aerodynamic diameters ranging between 1.6 and 15.8 μm. The percentage quoted is the fraction of all aerosol particles that pass through the glottis. (From Ref. 129.)

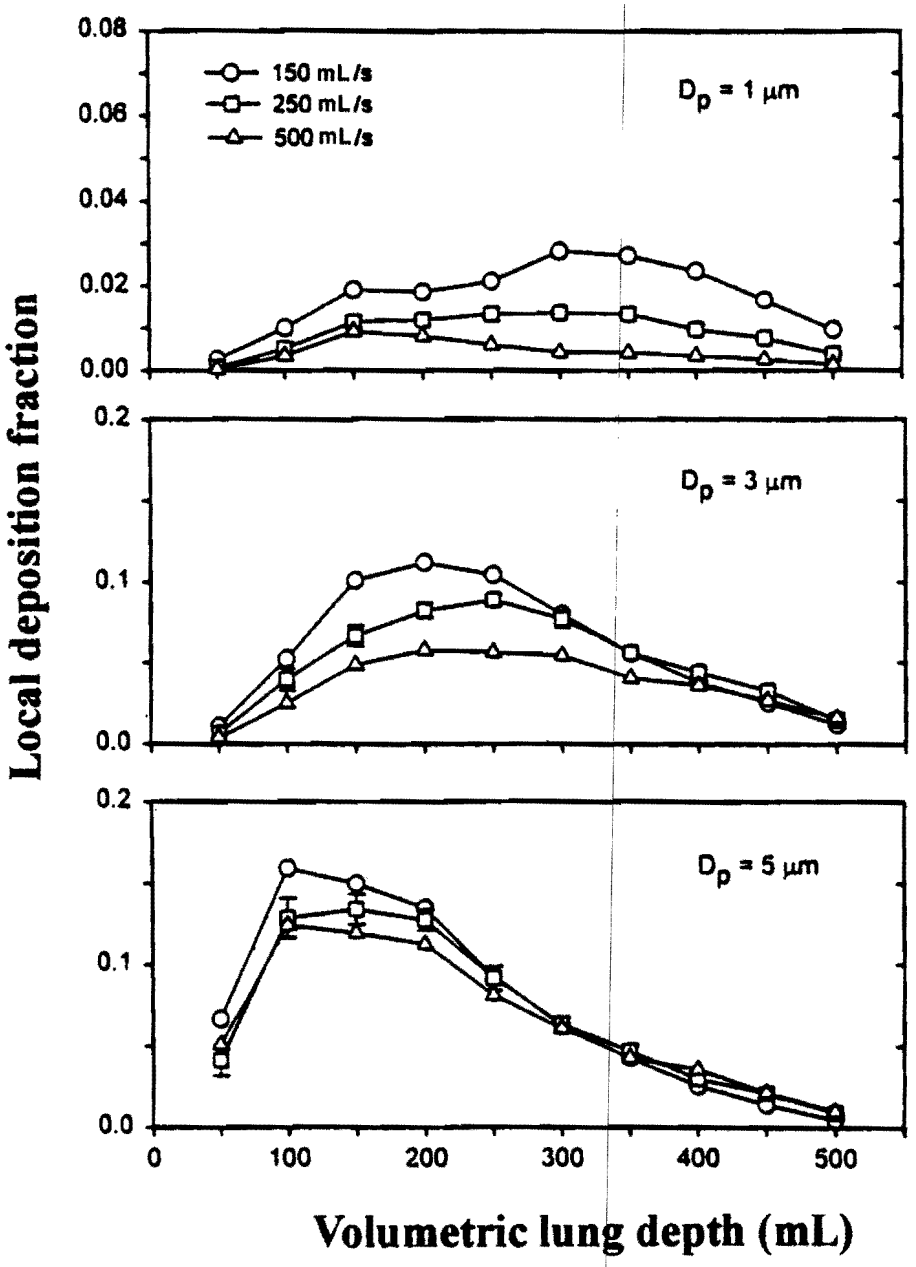

Figure 15 Experimental data on local deposition fraction from 11 young adults: Deposition fractions of 1-, 3-, and 5-μm particles are shown for ten volumetric lung compartments in lung depths between 50 and 500 cm^3. A tidal volume of 500 cm^3 was inhaled from functional residual capacity at flow rates of 150, 250, and 500 $cm^3\ s^{-1}$. Error bars (±SE) are shown for a flow rate of 250 $cm^3\ s^{-1}$. (From Ref. 67.)

was extremely uneven among the tube sections of the models. During inhalation, major deposition occurred in those daughter tube sections adjacent to the bifurcation. With increasing particle size or flow rate, deposition within these daughter sections increased from 70 to 90% of the total amount deposited in the model. During exhalation, peak deposition occurred again in those sections adjacent to the bifurcation, but now mainly in the adjacent parent tube section. This high surface density of particle deposition at bifurcations holds not only for coarse particles with impaction-determined deposition, but was also observed for ultrafine particles (105). For ultrafine particles, however, density differences between bifurcations and along the airway lengths were not so profound.

Spatial deposition patterns within airway bifurcations have been studied numerically (151–153,158; see Sec. IV.B, under Mathematical Models). Corresponding to the airway bifurcation models applied experimentally by Kim and coworkers, airway bifurcation geometries were constructed in a three-dimensional computer mesh and deposition patterns inferred from modeled airflow fields and particle trajectories. In general, there was a good agreement between the experimental results and the theoretical predictions. As an example, Figure 16 shows modeled deposition sites of 2000 randomly selected 5-μm particles (ρ = 0.891 g cm^{-3}) inhaled at a flow rate of 133 cm^3 s^{-1}. The parent branch has a diameter of 0.5 cm and the geometry of the bifurcation is symmetrical relative to daughter diameter (0.4 cm) and branching angle (45°), but flow division was changed from symmetrical to asymmetrical, with Q_{dA}/Q_{dB} being the ratio of flows rates in daughter branches A and B. For symmetrical flow division, the deposition pattern also appeared to be symmetrical. Most of the inhaled particles deposited as a hot-spot near the carina, but some particles were also found at the inner airway length of daughter branches. As the flow rate increased in daughter branch A relative to that in daughter branch B, the intensity and extension of the hot-spot in daughter branch A increased. With increasing asymmetry of flow division, the hot-spot in daughter B seemed first to recede to the carina, but then another hot-spot began to develop in the center of that daughter branch (see Fig. 16). These studies show that a homogeneous surface density of deposited particles within the tracheobronchiolar airways appears to be unrealistic. The given example may further illustrate the variability in deposition patterns and the complex mechanisms determining the site of particle deposition within an airway bifurcation.

However, more recent studies suggest (158,160–162,234) that flow regimens and particle trajectories crucially depend on the geometric boundary conditions, so that unrealistic deposition patterns may occur in simplified and idealized airway structures. This has to be disproved or verified in future studies, but it appears reasonable that coming studies must focus their interest on experimentally and numerically determined deposition patterns within realistic airway sys-

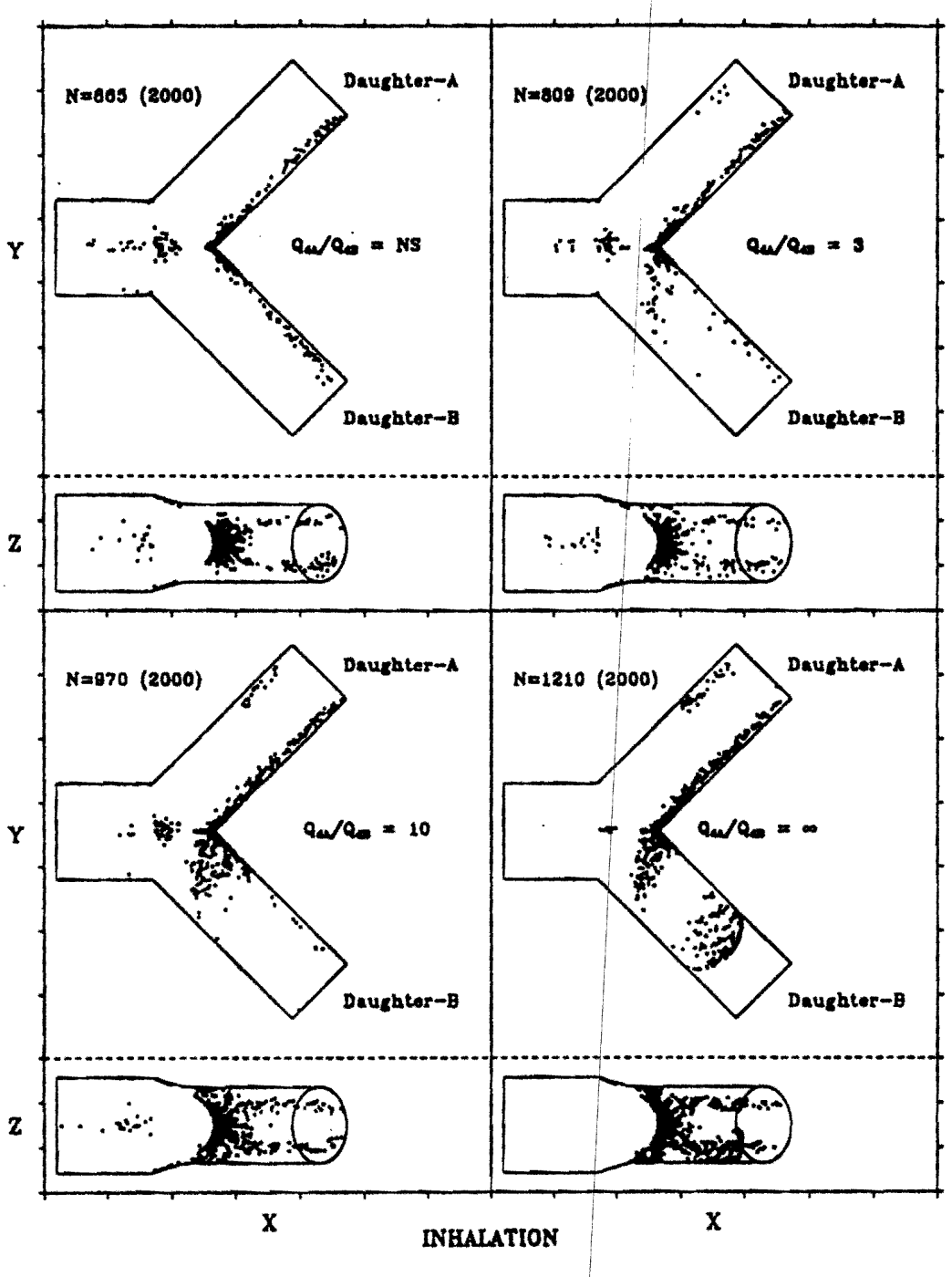

Figure 16 Modeled local deposition patterns in idealized airway structures: The effect of asymmetry in flow division on inspiratory deposition patterns of 5-μm particles (σ = 0.891 g cm^{-3}) is shown for four different flow–rate ratios between daughter branch A and branch B. (From Ref. 153.)

tems, especially because these approaches have now become available with modern computational techniques (159–162).

Nomenclature

CMD	count median diameter of a particle number frequency distribution (μm)
CF	correction factor applied for gender [see Eqs. (14) and (17)]
C_s	Cunningham slip correction factor
C(V)	particle number concentration of the respired volume (cm^{-3})
DE	deposition fraction; particles deposited in a given structure, as a fraction of all particles entering the respiratory system
DE_{Tot}	total deposition
DE_{ET}	extrathoracic deposition
$DE_{ET\text{-}N}$	extrathoracic deposition for nose breathing
$DE_{ET\text{-}M}$	extrathoracic deposition for mouth breathing
DE_{TB}	tracheobronchiolar deposition
DE_A	alveolar deposition
D_P	diffusion coefficient of a particle ($cm^2\ s^{-1}$)
D_p/Q	diffusion parameter (cm^{-1})
d	geometric particle diameter (μm)
d_{ae}	aerodynamic particle diameter (μm)
d_{th}	thermodynamic particle diameter (μm)
d_{16}	particle diameter at the 16% size cut of the cumulative particle size frequency distribution
d_{84}	particle diameter at the 84% size cut of the cumulative particle size frequency distribution
d_{ae}/Q	impaction parameter (μm s cm^{-3})
FRC	functional residual capacity, gas volume in the lung at the end of a normal expiration (cm^3)
G	factor characterizing the geometry of an obstacle (m)
g	gravity constant (9.81 m s^{-2})
MD	median particle diameter of a particle size frequency distribution (μm)
MMD	mass median diameter of a particle mass frequency distribution (μm)
Q	respiratory flow rate ($cm^3\ s^{-1}$)
SMD	surface median diameter of a particle surface frequency distribution (μm)
Stk	Stokes' number
T	absolute temperature (K)
t_a	residence time of particles in the alveolar region (s)
t_b	residence time of particles in the small bronchial airways (s)
t_{rs}	residence time of particles in the respiratory system (s)
u	linear airflow velocity (m s^{-1})
$V_{b\text{-}FRC}$	volume of the bronchioles at FRC level (cm^3)
V_{ET}	extrathoracic airway volume (cm^3)
V_{ex}	expired volume (cm^3)
V_{in}	inspired volume (cm^3)

V_T	tidal volume (cm^3)
Δ	root mean square diffusional displacement of particles ($cm\ s^{-1}$)
E	particle collection efficiency; particles deposited in a given structure as a fraction of all particles entering that structure
E_{ET}	particle collection efficiency of the extrathoracic airways
$E_{ET\text{-}N}$	extrathoracic particle collection efficiency for nose breathing
$E_{ET\text{-}M}$	extrathoracic particle collection efficiency for mouth breathing
E_{TB}	particle collection efficiency of the tracheobronchiolar region
E_A	particle collection efficiency of the alveolar region
η	dynamic viscosity of the surrounding medium ($kg\ s^{-1}\ m^{-1}$)
κ	Boltzmann constant ($1.38 \times 10^{-23}\ J\ K^{-1}$)
λ	mean free path of gas molecules (μm)
σ	gas density ($kg\ m^{-3}$)
σ_g	geometric standard deviation of a log-normal particle size distribution
ν	terminal settling velocity of a particle ($\mu m\ s^{-1}$)
ρ	particle density ($kg\ m^{-3}$)

References

1. Heyder J, Blanchard JD, Feldman HA, Brain JD. Convective mixing in human respiratory tract: estimates with aerosol boli. J Appl Physiol 1988; 64:1273–1278.
2. Paiva M, Engel L. Gas mixing in the lung periphery. In: Chang HK, Paiva M, eds. Respiratory Physiology. An Analytical Approach. New York: Marcel Dekker, 1989:245–276.
3. Schulz H, Heilmann P, Hillebrecht A, Gebhart J, Meyer M, Piiper J, Heyder J. Convective and diffusive gas transport in canine intrapulmonary airways. J Appl Physiol 1992; 72:1557–1562.
4. Ultmann JS. Gas transport in the conducting airways. In: Engel L, Paiva M, eds. Gas Mixing and Distribution in the Lung. New York: Marcel Dekker, 1985:63–136.
5. Weibel ER. Morphometry of the Human Lung. Heidelberg: Springer Verlag, 1963.
6. Breysse P, Swift DL. Inhalability of large particles into the human nasal passage: in vivo studies in still air. Aerosol Sci Technol 1990; 13:459–464.
7. Ménache MG, Miller FJ, Raabe OG. Particle inhalability curves for humans and small laboratory animals. Ann Occup Hyg 1995; 39:317–328.
8. Schlesinger RB. Biological disposition of airborne particles: basic principles and application to vehicular emissions. In: Watson AY, Bates RR, Kennedy D, eds. Air Pollution, the Automobile, and Public Health. Washington, DC: National Academy Press, 1988:239–298.
9. Swift DL. Design of the human respiratory tract to facilitate removal of particles and gases. AICh E Symp Ser 1976; 72(156):137–144.
10. Heyder J. Particle transport onto human airway surfaces. Eur J Respir Dis 1982; 63(suppl 119):29–50.
11. Geiser M, Baumann M, Cruz-Orive LM, Im Hof V, Waber U, Gehr P. The effect of particle inhalation on macrophage number and phagocytic activity in the intrapul-

monary conducting airways of hamsters. Am J Respir Cell Mol Biol 1994; 10:594–603.
12. Fuchs, NA. The Mechanics of Aerosols. New York: Dover Publications, 1989.
13. Hinds WC. Aerosol Technology. New York: John Wiley and Sons, 1982.
14. Willeke K, Baron, PA. Aerosol Measurement. Principles Techniques and Applications. New York: van Nostrand Reinhold, 1992:23–40.
15. Allan MD, Raabe OG. Slip correction measurements of spherical solid aerosol particles in an improved Milikan apparatus. Aerosol Sci Technol 1985; 4:69–86.
16. Gebhart J, Heyder J, Stahlhofen W. Use of aerosols to estimate pulmonary airspace dimensions. J Appl Physiol 1981; 51:465–476.
17. Chang HK. General concepts of molecular diffusion. In: Engel LA, Paiva M, eds. Gas Mixing and Distribution in the Lung. New York: Marcel Dekker, 1985:1–22.
18. Heyder J, Scheuch G. Diffusional transport of nonspherical aerosol particles. Aerosol Sci Technol 1983; 2:41–44.
19. Scheuch G, Heyder J. Dynamic shape factor of nonspherical aerosol particles in the diffusion regime. Aerosol Sci Technol 1990; 12:270–277.
20. Einstein A. On the kinetic molecular theory of thermal movements of particles suspended in a quiescent fluid. Ann Phys 1905; 17:549–560.
21. Asgharian B, Yu CP. Deposition of inhaled fibrous particles in the human lung. J Aerosol Med 1988; 1:37–50.
22. Asgharian B, Yu CP. Deposition of fibers in the rat lung. J Aerosol Sci 1989; 20: 355–366.
23. Timbrell V. An aerosol spectrometer and its applications. In: Mercer TT, Morrow PE, Stöber W, eds. Assessment of Airborne Particles. Springfield IL: CC Thomas, 1972:290–330.
24. Yu CP. Theories of electrostatic lung deposition of inhaled aerosols. Ann Occup Hyg 1985; 29:219–227.
25. Melandri C, Tarroni G, Prodi V, de Zaiacomo T, Formignani M, Lombardi CC. Deposition of charged particles in the human airways. J Aerosol Sci 1983; 14:657–669.
26. Jones AD, Johnston AM, Vincent JH. Static electrification of airborne asbestos dust. In: Marple VA, Liu BYH, eds. Aerosols in the Mining and Work Environment. Ann Arbor, MI: Ann Arbor Science, 1983:613–631.
27. Jones AD, Vincent JH, Johnston AM, McMillin CH. Effects of electrostatic charge on the pulmonary deposition of mineral dust aerosols inhaled by rats. J Aerosol Sci 1988; 19:565–575.
28. Vincent JH, Johnston WB, Jones AD, Johnston AM. Static electrification of airborne asbestos: a study of its causes, assessment and effects on deposition in the lungs of rats. Am Ind Hyg Assoc J 1981; 42:711–721.
29. Cohen BS, Xiong JQ, Li W. The influence of charge on the deposition behaviour of aerosol particles with emphasis on single charged nanometer sized particles. In: Marijnissen JCM, Gradon L, eds. Aerosol Inhalation: Recent Research Frontiers. Dordrecht: Kluwer Academic, 1996:153–164.
30. Stahlhofen W, Gebhart J, Rudolf G, Scheuch G. Measurement of lung clearance with pulses of radioactively labelled particles. J Aerosol Sci 1986; 17:333–336.

31. Stahlhofen W, Scheuch G, Bailey MR. Investigations of retention of inhaled particles in the human bronchial tree. Radiat Prot Dosim 1995; 60:311–319.
32. Scheuch G, Stahlhofen W, Heyder J. An approach to deposition and clearance measurements in human airways. J Aerosol Med 1996; 9:35–41.
33. Everard ML. Studies using radiolabelled aerosols in children. Thorax 1994; 49: 1259–1266.
34. Diot P, Baulieu J-L, Lemarié E. Nuclear medicine and lung diseases. Paris: Springer Verlag, 1993.
35. Rosenthal MS, Cullom J, Hawkins W, Moore SC, Tsui BMW, Yester M. Quantitative SPECT imaging: a review and recommendations by the Focus Committee of the Society of Nuclear Medicine Computer and Instrumentation Council. J Nucl Med 1995; 36:1489–1513.
36. Chan HK. Use of photon emission computed tomography in aerosol studies. J Aerosol Med 1993; 6:23–36.
37. Ferron GA, Erbe F, Fürst G, Haider B, Haller J, Köhl B, Kreyling WG, Schumann G, Stocker M, Heyder J. A scintillation counter for measuring removal of radioactive particles from dog lungs. J Aerosol Sci 1989; 20:1297–1300.
38. Gonda I. Scintigraphic techniques for measuring in vivo deposition. J Aerosol Med 1996; 9:S59–S67.
39. Itoh H, Smaldone GC, Swift DL, Wagner HN. Quantitative measurement of total aerosol deposition: comparison of three different techniques. J Aerosol Sci 1985; 16:367–371.
40. Morsey SM, Eckhardt B, Stahlhofen W, Pohlit W. Optimization studies of a whole-body counter to cope with possible dynamic transfer between neighboring compartments. Health Phys 1978; 35:325–332.
41. Smaldone GC. Factors in measurement of dose by gamma scintigraphy. J Aerosol Med 1996; 9:S69–S76.
42. Stahlhofen W, Gebhart J, Heyder J. Experimental determination of the regional deposition of aerosol particles in the human respiratory tract. Am Ind Hyg Assoc J 1980; 41:385–398.
43. Suzuki S. Detection efficiency of NaI (Tl) crystals and loss of positron resolution caused by photon interactions in the crystals in γ-cameras. Int J Appl Radiat Isot 1982; 33:411–414.
44. Boecker BB, Thomas RG, McClellan RO. Accumulation and retention of 137-Cs fused aluminiosilicate particles by beagle dogs after repeated inhalation exposures. In: Walton WH, ed. Inhaled Particles IV. Oxford: Pergamon, 1977:551–561.
45. Cuddihy RG, Boecker BB. Controlled administration of respiratory tract burdens of inhaled radioactive aerosols in beagle dogs. Toxicol Appl Pharmacol 1973; 25: 597–605.
46. Morrow PE, Gibb FR, Johnson L. Clearance of insoluble dust from the lower respiratory tract. Health Phys 1964; 10:543–555.
47. Heyder J, Gebhart J, Stahlhofen W. Inhalation of aerosols: particle deposition and retention. In: Willeke K, ed. Generation of Aerosols and Facilities for Exposure Experiments. Ann Arbor, MI: Ann Arbor Scientific, 1980:65–103.
48. Stahlhofen W. Human data on deposition. In: Smith H, Gerber G, eds. Lung Model-

ling for Inhalation of Radioactive Materials. Commission of the European Communities. 1984:39–62.
49. Fleming JS, Nassim M, Hashish AH, Bailey AG, Conway J, Holgate S, Halson P, Moore E, Martonen TB. Description of pulmonary deposition of radiolabeled aerosol by airway generation using a conceptual three dimensional model of lung morphology. J Aerosol Med 1995; 8:341–356.
50. Newman SP, Pavia D. Aerosol deposition in man. In: Móren F, Newhouse MT, Dolovich MB, eds. Aerosols in Medicine. Principles, Diagnosis and Therapy. Amsterdam: Elsevier, 1993:193–217.
51. Anderson PJ, Dolovich MB. Aerosols as diagnostic tools. J Aerosol Med 1994; 7: 77–88.
52. Agnew JE. Characterizing lung aerosol penetration. J Aerosol Med 1991; 4:237–249.
53. Dolovich MB, Sanchis J, Rossman C, Newhouse MT. Aerosol penetrance: a sensitive index of peripheral airway obstruction. J Appl Physiol 1976; 40: 468–471.
54. Phipps PR, Gonda I, Bailey D, Borham P, Bautovich G, Anderson SD. Comparison of planar and tomographic gamma scintigraphy to measure the penetration index of inhaled aerosols. Am Rev Respir Dis 1989; 139:1516–1523.
55. Schuster DP. Positron emission tomography: theory and its application to study of lung disease. Am Rev Respir Dis 1989; 139:818–840.
56. Cohen D. Ferrimagnetic contamination in the lungs and other organs of the human body. Science 1973; 180:745–748.
57. Cohen D, Crowther TS, Gibbs GW, Becklake MR. Magnetic lung measurements in relation to occupational exposure in asbestos miners and millers in Quebec. Environ Res 1981; 26:535–550.
58. Freedman AP, Robinson SE. Evaluation of magnetopneumography for assessing thoracic accumulation of welding fume. In: Erné SN, Hahlbohm HD, Lübbig H, eds. Biomagnetism. Berlin: Walter de Gruyter, 1981:489–495.
59. Kalliomäki PL, Karp PK, Katila T, Makipaw P, Jaar P, Tossavainen A. Magnetic measurements of pulmonary contamination. Scand J Work Environ Health 1976; 4:232–239.
60. Stahlhofen W, Möller M. Behaviour of magnetic micro-particles in the human lung. Radiat Environ Biophys 1993; 32:221–238.
61. Valberg PA, Brain JD. Generation and use of three types of iron oxide aerosol. Am Rev Respir Dis 1979; 120:1013–1024.
62. Möller W, Stahlhofen W, Roth C. Improved spinning top aerosol generator for the production of high concentrated ferrimagnetic aerosols. J Aerosol Sci 1990; 21: S435–S438.
63. Brain JD, Bloom SB, Valberg PA, Gehr P. Correlation between the behavior of magnetic iron oxide particles in the lungs of rabbits and phagocytosis. Exp Lung Res 1984; 6:115–131.
64. Freedman AP, Robinson SE, Street MR. Magnetopneumographic study of human alveolar clearance in health and disease. Ann Occup Hyg 1988; 32:809–820.
65. Tyndall J. Essays on the Floating Matter of the Air. London: Longmans Green, 1881.
66. Altshuler B, Yarmus L, Palmes ED, Nelson N. Aerosol deposition in the human

respiratory tract. I. Experimental procedures and total deposition. AMA Arch Ind Health 1957; 15:293–303.
67. Kim CS, Hu SC, DeWitt P, Gerrity TR. Assessment of regional deposition of inhaled particles in human lungs by serial bolus delivery method. J Appl Physiol 1996; 81:2203–2213.
68. Palmes ED, Wang CS. An aerosol inhalation apparatus for human single breath deposition studies. Am Ind Hyg Assoc J 1971; 32:43–46.
69. Giacomelli-Maltoni G, Melandri C, Prodi V, Tarroni G. Deposition efficiency of monodisperse particles in human respiratory tract. Am Ind Hyg Assoc J 1972; 33: 603–610.
70. Heyder J, Armbruster L, Gebhart J, Grein E, Stahlhofen W. Total deposition of aerosol particles in the human respiratory tract for nose and mouth breathing. J Aerosol Sci 1975; 6:311–329.
71. Heyder J, Gebhart J, Stahlhofen W, Stuck B. Biological variability of particle deposition in the human respiratory tract during controlled and spontaneous mouth-breathing. Ann Occup Hyg 1982; 26:137–147.
72. Heyder J, Gebhart J, Scheuch G. Influence of human lung morphology on particle deposition. J Aerosol Sci 1988; 1:81–88.
73. Gebhart J, Heigwer G, Heyder J, Roth C, Stahlhofen W. The use of light scattering photometry in aerosol medicine. J Aerosol Med 1988; 1:89–112.
74. Im Hof V, Scheuch G, Geiser M, Gebhart J, Gehr P, Heyder J. Techniques for the determination of particle deposition in lungs of hamsters. J Aerosol Med 1989; 2: 247–259.
75. Schulz H, Schulz A, Heyder J. Influence of intrinsic particle properties on parameters of aerosol bolus dispersion. Exp Lung Res 1996; 22:393–407.
76. Westenberger S, Gebhart J, Jaser S, Knoch M, Köstler R. A novel device for the generation and recording of aerosol micro-pulses in lung diagnostics. J Aerosol Sci 1992; 23:S449–S452.
77. Heyder J, Blanchard JD, Brain JD. Particle deposition in volumetric regions of the human respiratory tract. Ann Occup Hyg 1988; 32:71–79.
78. Brand P, Scheuch G, Schulz H, Meyer T, Kohlhäufl M, Heyder J, Häussinger K. Ermittlung der Verteilung inhalierter Aerosolteilchen mit der Aerosolbolustechnik. In: Scheuch G, ed. Aerosole in der Inhalationstherapie. München-Deisenhofen: Dustri-Verlag, 1997:27–40.
79. Sweeney TD, Brain JD. Pulmonary deposition: determinants and measurement techniques. Toxicol Pathol 1991; 4:384–397.
80. Sweeney TD, Brain JD, LeMott S. Anesthesia alters the pattern of aerosol retention in hamsters. J Appl Physiol 1983; 54:37–44.
81. Valberg PA, Brain JD, Sneddon SL, LeMott SR. Breathing pattern influences aerosol deposition sites in excised dog lungs. J Appl Physiol 1982; 53:824–837.
82. Logan GR, Schnitt SJ, Dvorak AM. Rapid microwave fixation of human tissue for light microscopic immunoperoxidase identification of diagnostically useful antigens. Lab Invest 1987; 57:585–591.
83. Pinkerton KE, Gallen JT, Mercer RR, Wong VC, Plopper CG, Tarkington BK. Aerosolized fluorescent microspheres detected in the lung using confocal scanning laser microscopy. Microsc Res Technol 1993; 26:437–443.

84. Godleski JJ, Hastings CL, Katler M, Sweeney TD. Preservation of the relationship of airway mucus and epithelium by slam freezing. In: Baily GW, ed. Proceedings of the 49th Annual Meeting of the Electron Microscopy Society of America. San Francisco: San Francisco Press, 1991:72–73.
85. Brain JD, Knudson DE, Sorokin SP, Davis MA. Pulmonary distribution of particles given by intratracheal instillation or by aerosol inhalation. Environ Res 1976; 11: 13–33.
86. Sweeney TD, Brain JD, Tryka AF, Godleski JJ. Retention of inhaled particles in hamsters with pulmonary fibrosis. Am Rev Respir Dis 1983; 128:138–143.
87. Herz RH. The Photographic Action of Ionizing Radiations. New York: Wiley-Interscience, 1969.
88. Rogers AW. Techniques of Autoradiography. New York: Elsevier, 1978.
89. Sweeney TD, Skornik WA, Brain JD, Hatch V, Godleski JJ. Chronic bronchitis alters the pattern of aerosol deposition in the lung. Am J Respir Crit Care Med 1995; 151:482–488.
90. Geiser M, Im Hof V, Gehr P, Cruz-Orive LM. Histological and stereological analysis of particle retention in the conducting airways of hamster lungs. J Aerosol Med 1990; 3:131–145.
91. Geiser M, Cruz-Orive LM, Waber U, Im Hof V, Gehr P. Particle retention in airways estimated by unbiased stereology and photometry. J Aerosol Sci 1995; 8: 149–165.
92. Sweeney TD, Blanchard JD, Carter JE, Brain JD. Delivery of aerosolized drugs to the lungs with a metered dose inhaler: quantitative analysis of regional deposition. J Aerosol Sci 1990; 21:350–351.
93. Zeltner TB, Sweeney TD, Skornik WA, Feldman HA, Brain JD. Retention and clearance of 0.9 μm particles inhaled by hamsters during rest or exercise. J Appl Physiol 1991; 70:1137–1145.
94. Kreyling WG, Blanchard JD, Godleski JJ, Häussermann S, Heyder J, Hutzler P, Schulz H, Sweeney TD, Takenaka S. Shallow aerosol bolus inhalation in beagle dogs: sites of retention and clearance. Eur Respir J 1995; 8:352S.
95. Godleski JJ, Stearns RC, Katler M, Hastings CL. Detection of elements by electron spectroscopic imaging and analysis of electron energy loss spectra in alveolar macrophages prepared by slam-freeze molecular distillation processing. EMSA Proc 1990; 48:776–777.
96. Godleski JJ, Kreyling WG. Localisation of cobalt in the matrix of airway cartilage. Am Rev Respir Dis 1990; 141:A525.
97. Bell KA, Friedländer SK. Aerosol deposition in models of a human lung bifurcation. Staub Reinhalt Luft 1973; 33:178–182.
98. Kim CS, Iglesias AJ. Deposition of inhaled particles in bifurcating airway models: I. Inspiratory deposition. J Aerosol Med 1989; 2:1–14.
99. Kim CS, Iglesias AJ, Garcia L. Deposition of inhaled particles in bifurcating airway models: II. Expiratory deposition. J Aerosol Med 1989; 2:15–27.
100. Kim CS, Fisher DM, Lutz DJ, Gerrity TR. Particle deposition in bifurcating airway models with varying airway geometry. J Aerosol Sci 1994; 25:567–581.
101. Kinsara AA, Loyalka SK, Tompson RV, Miller WH, Holub RF. Deposition patterns

of molecular phase radon progeny (^{218}Po) in lung bifurcations. Health Phys 1995; 68:371–382.
102. Martonen TB, Hofmann W, Lowe JE. Cigarette smoke and lung cancer. Health Phys 1987; 52:213–217.
103. Lee WC, Wang CS. Particle deposition in a system of repeatedly bifurcating tubes. In: Walton WH, ed. Inhaled Particles IV. Oxford: Pergamon Press, 1977:49–59.
104. Guilmette RA, Gagliano TJ. Construction of a model of human nasal airways using in vivo morphometric data. Ann Occup Hyg 1994; 38(suppl 1):69–75.
105. Cohen BS, Sussman RG, Lippmann M. Ultrafine particle deposition in a human tracheobronchial cast. Aerosol Sci Technol 1990; 12:1082–1091.
106. Yamada Y, Cheng YS, Yeh HC, Swift DL. Inspiratory and expiratory deposition of ultrafine particles in a human nasal cast. Inhal Toxicol 1988; 1:1–11.
107. Yamada Y, Koizumi A, Fukuda S, Inaba J, Cheng YS, Yeh HC. Deposition of ultrafine monodisperse particles in a human tracheobronchial cast. Ann Occup Hyg 1994; 38(suppl 1):91–100.
108. Cheng YS, Yamada Y, Yeh HC, Swift DL. Diffusional deposition of ultrafine aerosols in a human nasal cast. J Aerosol Sci 1988; 19:741–751.
109. Cheng YS, Yamada Y, Yeh HC, Swift DL. Deposition of ultrafine aerosols in a human oral cast. Aerosol Sci Technol 1990; 12:1075–1081.
110. Martonen TB, Lowe J. Assessment of aerosol deposition patterns in human respiratory tract casts. In: Marple VA, Lui BYH, eds. Aerosols in the Mining and Industrial Work Environments: Fundamentals and Status. Ann Arbor, MI: Ann Arbor Science, 1983: 151–164.
111. Schlesinger RB, Lippmann M. Selective particle deposition and bronchogenic carcinoma. Environ Res 1978; 15:424–431.
112. Swift DL, Montassier N, Hopke PK, Karpen-Hayes K, Cheng YS, Su YF, Yeh HC, Strong JC. Inspiratory deposition of ultrafine particles in human nasal replicate cast. J Aerosol Sci 1992; 23:65–72.
113. Heyder J, Rudolf G. Mathematical models of particle deposition in the human respiratory tract. J Aerosol Sci 1984; 15:697–707.
114. Morrow PE, Yu CP. Models of aerosol behavior in airways. In: Móren F, Newhouse MT, Dolovich MB, eds. Aerosols in Medicine. Principles, Diagnosis and Therapy. Amsterdam: Elsevier, 1993:157–193.
115. Hofmann W. Lung morphometry and particle transport and deposition: overview of existing models. In: Marijnissen JCM, Gradon L, eds. Aerosol Inhalation: Recent Research Frontiers. Dordrecht: Kluwer Academic, 1996:91–102.
116. Swift DL. Use of mathematical aerosol deposition models in predicting the distribution of inhaled therapeutic aerosols. In: Hickey A, ed. Inhalation Aerosols: Physical and Biological Basis for Therapy. New York: Marcel Dekker, 1996:51–81.
117. Findeisen W. Über das Absetzen kleiner, in der Luft suspendierter Teilchen in der menschlichen Lunge bei der Atmung. Pflügers Arch Physiol 1935; 236:367–379.
118. Altshuler B. Calculation of regional deposition of aerosol in the respiratory tract. Bull Math Biophys 1959; 21:257–270.
119. Taulbee DB, Yu CP. A theory of aerosol deposition in the human respiratory tract. J Appl Physiol 1975; 38:77–85.

120. Scott WR, Taulbee DB, Yu CP. Theoretical study of nasal deposition. Bull Math Biol 1978; 40:581–603.
121. Landahl HD. On the removal of air-borne droplets by the human respiratory tract: I. The lung. Bull Math Biophys 1950; 12:43–56.
122. Landahl HD. Particle removal by the respiratory system: note on the removal of airborne particulates by the human respiratory tract with particular reference to the role of diffusion. Bull Math Biophys 1963; 25:29–37.
123. Beeckmans JM. Correction factor for size-selective sampling, results based on a new computed alveolar deposition curve. Ann Occup Hyg 1965; 8:221–231.
124. Beeckmans JM. The deposition of aerosols in the respiratory tract. I. Mathematical analysis and comparison with experimental data. Can J Physiol Pharmacol 1965; 43:157–172.
125. Beeckmans JM. Deposition of asbestos particles in the human respiratory tract. Int Environ Stud 1970; 1:31–34.
126. ICRP Task Group on Lung Dynamics. Deposition and retention models for internal dosimetry of the human respiratory tract. Health Phys 1966; 10:1163–1174.
127. Mitchel RE. Aerosol retention in the lungs as a function of respiration rate and particle size. Ph.D. dissertation. Ohio State University, 1971.
128. Harris RL, Fraser DA. A model for deposition of fibers in the human respiratory system. Am Ind Hyg Assoc J 1976; 37:73–89.
129. Gerrity TR, Lee PS, Haas FJ, Marinelli A, Werner P, Lourenco RV. Calculated deposition of inhaled particles in the airway generations of normal subjects. J Appl Physiol 1979; 47:867–873.
130. Gerrity TR, Garrard CS, Yeates DB. Theoretic analysis of sites of aerosol deposition in the human lung. Chest 1981; 80:898–901.
131. Yeh HC, Schum GM. Models of human lung airways and their application to inhaled particle deposition. Bull Math Biol 1980; 42:461–480.
132. Hofmann E, Steinhäuser F, Pohl E. Dose calculations for the respiratory tract from inhaled natural radioactive nuclides as a function of age. Health Phys 1979; 37: 517–532.
133. Hofmann W, Koblinger L. Monte Carlo modeling of aerosol deposition in human lungs. Part II: Deposition fractions and their sensitivity to parameter variations. J Aerosol Sci 1990; 21:675–688.
134. Hofmann W, Koblinger L. Monte Carlo modeling of aerosol deposition in human lungs. Part III: Comparison with experimental data. J Aerosol Sci 1992; 23:51–63.
135. Phalen RF, Oldham MJ, Kleinman MT, Crocker TT. Tracheobronchial deposition predictions for infants, children, and adolescents. Ann Occup Hyg 1988; 32:11–21.
136. Phalen RF, Cuddihy RG, Fisher GL, Moss OR, Schlesinger RB, Swift DL, Yeh HC. Main features of the proposed NCRP respiratory tract model. Radiat Prot Dosim 1991; 38:179–184.
137. Yeh HS, Cuddihy RG, Phalen RB, Chang IY. Comparison of calculated respiratory tract deposition of particles based on the proposed NCRP model and the new ICRP66 model. Aerosol Sci Technol 1996; 25:134–140.
138. ICRP Publication 66. Human Respiratory Tract Model for Radiological Protection. New York: Elsevier Science, 1994.

139. Altshuler B, Nelson N, Kuschner M. Estimation of lung tissue dose from the inhalation of radon and daughters. Health Phys 1964; 10:1137–1161.
140. Altshuler B, Palmes ED, Nelson N. Regional aerosol deposition in the human respiratory tract. In: Davies CN, ed. Inhaled Particles and Vapours II. Oxford: Pergamon Press, 1967:323–337.
141. Scherer PW, Shendalman LH, Greene NM. Simultaneous diffusion and convection in single breath lung washout. Bull Math Biophys 1972; 34:393–412.
142. Olson DE, Dart GE, Filley GF. Pressure drop and fluid flow regime of air inspired into the human lung. J Appl Physiol 1970; 28:482–494.
143. Taulbee DB, Yu CP, Heyder J. Aerosol transport in the human lung from analysis of single breaths. J Appl Physiol 1978; 44:803–812.
144. Crawford DJ. Identifying critical human subpopulations by age groups: radioactivity and the lung. Phys Med Biol 1982; 27:539–552.
145. Yeh HC, Hulbert AJ, Phalen RF, Raabe OG. Mathematical considerations for particle deposition in the tracheobronchial tree: equations and lung model. LF-49 Inhalation Toxicology Research Institute Annual Report. Albuquerque, NM; Lovelace Foundation for Medical Education and Research, 1979.
146. Koblinger L, Hofmann W. Analysis of human lung morphometric data for stochastic aerosol deposition calculations. Phys Med Biol 1985; 30:541–556.
147. Koblinger L, Hofmann W. Monte Carlo modeling of aerosol deposition in human lungs. Part I: Simulation of particle transport in a stochastic lung structure. J Aerosol Sci 1990; 21:661–674.
148. Ferron GA, Hornik S, Kreyling WG, Haider B. Comparison of experimental and calculated data for the total and regional deposition in the human lung. J Aerosol Sci 1985; 16:133–143.
149. Hofmann W, Mainelis G. A comparative study of submicron particle deposition in human lungs. J Aerosol Sci 1993; 24:S359–S360.
150. Yu CP, Diu CK. A comparative study of aerosol deposition in different lung models. Am Ind Hyg Assoc J 1982; 43:54–65.
151. Balásházy I, Hofmann W. Particle deposition in airway bifurcations—I. Inspiratory flow. J Aerosol Sci 1993; 24:745–772.
152. Balásházy I, Hofmann W. Particle deposition in airway bifurcations—II. Expiratory flow. J Aerosol Sci 1993; 24:773–786.
153. Balásházy I, Hofmann W. Deposition of aerosols in asymmetric airway bifurcations. J Aerosol Sci. 1995; 26:273–292.
154. Gradon L, Orlicki D. Deposition of inhaled aerosol particles in a generation of the tracheobronchial tree. J Aerosol Sci, 1990; 21:3–19.
155. Li WI, Perzl M, Heyder J, Langer R, Brain JD, Englmeier KH, Niven RW, Edwards DA. Aerodynamics and aerosol particle deaggregation phenomena in model oral–pharyngeal cavities. J Aerosol Sci 1996; 27:1269–1286.
156. Katz IM, Martonen TB. Flow patterns in three-dimensional laryngeal models. J Aerosol Med 1996; 9:501–512.
157. Katz IM, Martonen TB. Three-dimensional fluid particle trajectories in the human larynx and trachea. J Aerosol Med 1996; 9:513–520.
158. Heistracher T, Hofmann W. Physiologically realistic models of bronchial airway bifurcations. J Aerosol Sci 1995; 26:497–509.

159. Perzl MA, Schulz H, Paretzke HG, Englmeier KH, Heyder J. Reconstruction of the lung geometry for the simulation of aerosol transport. J Aerosol Med 1986; 9: 409–418.
160. Perzl MA, Li W, Edwards DA, Tippe A, Lasser R, Schulz H, Heyder J. Three Dimensional Air Flow Simulations in Realistic Airway Geometries. Aerosol Med 1997; 10:254.
161. Tippe A, Häußermann S. In vitro measurements of flow within bronchial bifurcations. Eur J Physiol 1995; 430(suppl):R156.
162. Tippe A, Perzl MA, Li W, Schulz H. Flow in Bifurcation Models: Comparison Between Experiment and Numerical Simulation. Aerosol Med 1997; 10: 254.
163. Heyder J, Gebhart J, Rudolf G, Schiller CF, Stahlhofen W. Deposition of particles in the human respiratory tract in the size range 0.005–15 μm. J Aerosol Sci 1986; 17:811–825.
164. Cohen BS, Asgharian B. Deposition of ultrafine particles in the upper airways: an empirical analysis. J Aerosol Sci 1990; 21:789–797.
165. Rudolf G. A mathematical model for the deposition of aerosol particles in the human respiratory tract. J Aerosol Sci 1984; 15:195–199.
166. Rudolf G, Gebhart J, Heyder J, Scheuch G, Stahlhofen W. Modelling the deposition of aerosol particles in the human respiratory tract. J Aerosol Sci 1983; 14:188–192.
167. Rudolf G, Gebhart J, Heyder J, Schiller CF, Stahlhofen W. An empirical formula describing aerosol deposition in man for any particle size. J Aerosol Sci 1986; 17: 350–355.
168. Rudolf G, Köbrich R, Stahlhofen W. Modelling and algebraic formulation of regional aerosol deposition in man. J Aerosol Sci 1990; 21:S403–S406.
169. Schiller CF, Gebhart J, Heyder J, Rudolf G, Stahlhofen W. Factors influencing total deposition of ultrafine aerosol particles in the human respiratory tract. J Aerosol Sci 1986; 17:328–332.
170. Schiller CF, Gebhart J, Heyder J, Rudolf G, Stahlhofen W. Deposition of monodisperse insoluble aerosol particles in the 0.005 to 0.2 μm size range within the human respiratory tract. Ann Occup Hyg 1988; 32(suppl 1):41–49.
171. Anderson PJ, Hiller FC, Mazumder MK. Deposition of 0.02–0.2 μm particles in the human respiratory tract: effects of variations in respiratory pattern. Ann Occup Hyg 1988; 32(suppl 1):91–100.
172. Bennett WD. Human variation in spontaneous breathing deposition fraction: a review. J Aerosol Med 1988; 1:67–80.
173. Miller FJ, Martonen TB, Ménache MG, Graham RC, Spektor DM, Lippmann M. Influence of breathing mode and activity level on the regional deposition of inhaled particles and implications for regulatory standards. Ann Occup Hyg 1988:32(suppl 1):3–10.
174. Davies CN, Lever M, Rothenberg S. Experimental studies of the deposition of particles in the human lungs. In: Walton HA, ed. Inhaled Particles IV. Oxford: Pergamon 1977:151–162.
175. Bennett WD, Smaldone GC. Human variation in the peripheral air-space deposition of inhaled particles. J Appl Physiol 1987; 62:1603–1610.

176. Tobin MJ, Chadha TS, Jenouri G, Birch SJ, Gazeroglu K, Sackner MA. Breathing patterns 1. Normal subjects. Chest 1983; 84:202–205.
177. Shea SA, Walter J, Murphy K, Guz A. Evidence for individuality of breathing patterns in resting healthy man. Respir Physiol 1987; 68:331–344.
178. Swift DL, Proctor DF. A dosimetric model for particles in the respiratory tract above the trachea. Ann Occup Hyg 1988; 32(suppl 1):1035–1044.
179. Hahn I, Scherer PW, Mozell MM. Velocity profiles for airflow through a large-scale model of the human nose. J Appl Physiol 1993; 75:2273–2287.
180. Schlichting H. Boundary-Layer Theory (Trans. by Kestin J). Stanford: McGraw-Hill, 1968.
181. Cheng YS, Su YF, Yeh HC, Swift DL. Deposition of thoron progeny in human head airways. Aerosol Sci Technol 1993; 18:359–375.
182. Swift DL, Strong JC. Nasal deposition of ultrafine ^{218}Po aerosols in human subjects. J Aerosol Sci 1996; 27:1125–1132.
183. Fry FA, Black A. Regional deposition and clearance of particles in the human nose. Aerosol Sci 1973; 4:113–124.
184. Stahlhofen W, Rudolf G, James AC. Intercomparison of experimental regional aerosol deposition data. J Aerosol Med 1989; 2:285–308.
185. Cheng KH, Cheng YY, Yeh HC, Guilmette RA, Simpson SQ, Yang YH, Swift DL. In vivo measurements of nasal airway dimensions and ultrafine aerosol deposition in the human nasal and oral airways. J Aerosol Sci 1996; 27:785–801.
186. Guilmette RA, Wicks JD, Wolff RK. Morphometry of human nasal airways in vivo using magnetic resonance imaging. J Aerosol Med 1989; 2:365–377.
187. Rasmussen TR, Swift DL, Hilberg O, Pedersen OF. Influence of nasal passage geometry on aerosol particle deposition in the nose. J Aerosol Med 1990; 3:15–25.
188. Rudolf G. Deposition von Aerosolteilchen in der Nase. [Deposition of aerosol particles in the nose]. Dissertation. University Frankfurt/Main, Frankfurt, Germany, 1975.
189. Zhang L, Yuh CP. Empirical equations for nasal deposition of inhaled particles in small laboratory animals and humans. Aerosol Sci Technol 1993; 19:51–56.
190. Gradon L, Yu CP. Diffusional particle deposition in the human nose and mouth. Aerosol Sci Technol 1989; 11:213–220.
191. Emmett PC, Aitken RJ. Measurement of the total and regional deposition of inhaled particles in the human respiratory tract. J Aerosol Sci 1982; 13:549–560.
192. Bowes SM III, Swift DL. Deposition of inhaled particles in the oral airway during oronasal breathing. Aerosol Sci Technol 1989; 11:157–167.
193. Niinimaa V, Cole P, Mintz S, Shephard RJ. Oronasal distribution of respiratory airflow. Respir Physiol 1981; 43:69–75.
194. Swift DL, Cheng YS, Su YF, Yeh HC. Ultrafine aerosol deposition in the human nasal and oral passages. Ann Occup Hyg 1994; 38:77–81.
195. Ferron GA, Busch B, Gebhart J, Roth C. Evaporation of aerosols produced with eleven jet nebulizers. J Aerosol Sci 1996; 27:S381–S382.
196. Anderson M, Philipson K, Svartengren M, Camner P. Human deposition and clearance of 6-μm particles inhaled with an extremely low flow rate. Exp Lung Res 1995; 21:187–195.

197. Svartengren K, Philipson K, Svartengren M, Anderson M, Camner P. Tracheobronchial deposition and clearance in small airways in asthmatic subjects. Eur Respir J 1996; 9:1123–1129.
198. Phalen RF, Oldham MJ, Schum GM. Growth and ageing of the bronchial tree: implications for particle deposition calculations. Radiat Prot Dosim 1991; 38:15–21.
199. Hugonaud C, Gehr P, Weibel EW, Burri PH. Adaptation of the growing lung to increased oxygen consumption II. Morphometric analysis. Respir Physiol 1977; 29: 1–10.
200. Cudmore RE, Emery JL, Mithal A. Postnatal growth of the bronchi and bronchioles. Arch Dis Child 1962; 37:481–484.
201. Stocks J, Quanjar PH. Reference values for residual volume, functional residual capacity and total lung capacity. Eur Respir J 1995; 8:492–506.
202. DeGroodt EG, Quanjer PH, Wise ME, van Zomeren BC. Changing relationships between stature and lung volumes during puberty. Respir Physiol 1986; 65:139–153.
203. Hislop A, Muir DCF, Jacobsen M, Simon G, Reid L. Postnatal growth and function of the preacinar airways. Thorax 1072; 27:265–274.
204. Schrader PC, Quanjer PH, Olievier ICW. Respiratory muscle force and ventilatory function in adolescents. Eur Respir J 1988; 1:368–375.
205. Schrader PC, Quanjer PH, van Zomeren BC, Wise ME. Changes in the FEV_1–height relationship during pubertal growth. Bull Eur Physiopathol Respir 1984; 20: 381–388.
206. Schrader PT, Quanjer PH, Borsboom G, Wise ME. Evaluating lung function and antropometric growth data in a longitudinal study on adolescents. Hum Biol 1984; 56:365–381.
207. Buist AS, Gheo H, Anthonisen NR, Cherniack RM, Ducic S, Macklem PT, Manfreda J, Martin RR, McCarthy D, Ross BB. Relationship between single-breath N_2 test and age, sex, and smoking habit in three north American cities. Am Rev Respir Dis 1979; 120:305–318.
208. Bode FR, Dosman J, Martin RR, Gheo H, Macklem PT. Age and sex differences in lung elasticity and in closing capacity in nonsmokers. J Appl Physiol 1976; 41: 129–135.
209. Becklake M, Crapo RO. Lung function testing: selection of reference values and interpretative strategies. Am Rev Respir Dis 1991; 144:1202–1218.
210. Chiang ST, Wang BC, Chi YL, Hsieh YC. Ventilatory components of lungs in relation to sex and age. Am Rev Respir Dis 1971; 104:175–181.
211. Sherrill DL, Lebowitz MD, Knudson RJ, Burrows B. Continuous longitudinal regression equations for pulmonary function measures. Eur Respir J 1992; 5:452–462.
212. Becquemin MH, Roy M, Bouchikhi A, Teillac A. Deposition of inhaled particles in healthy children. In: Hofmann W, ed. Deposition and Clearance of Aerosols in the Human Respiratory Tract. Vienna: Facultas, 1987:22–27.
213. Becquemin MH, Yu CP, Roy M, Bouchikhi A. Total deposition of inhaled particles related to age: comparison with age-dependent model calculations. Radiat Prot Dosim 1991; 38:23–28.

214. Schiller-Scotland CF, Hlawa R, Gebhart J, Wönne R, Heyder J. Total deposition of aerosol particles in the respiratory tract of children during spontaneous and controlled mouth breathing. J Aerosol Sci 1992; 23:S457–S460.
215. Schiller-Scotland CF, Hlawa R, Gebhart J, Heyder J, Roth C. Wönne R. Particle deposition in the respiratory tract of children during spontaneous and controlled mouth breathing. Ann Occup Hyg 1994; 38(suppl 1):117–125.
216. Fok TF, Monkman S, Dolovich M, Gray S, Coates G, Paes B, Rashid F, Newhouse M, Kirpalani H. Efficiency of aerosol medication delivery from a metered dose inhaler versus jet nebulizer in infants with bronchopulmonary dysplasia. Pediatr Pulmonol 1996; 21:301–309.
217. Grigg J, Amon S, Jones T, Clarke A, Silverman M. Delivery of therapeutic aerosols to intubated babies. Arch Dis Child 1992; 67:25–30.
218. Wattenberg KL, Clark AR, Kelly HW, Murphy S. Delivery of aerosolised medication to intubated babies. Pediatr Pulmonol 1991; 10:136–141.
219. Arnon S, Grigg J, Nikander K, Silverman M. Delivery of micronized budesonide suspension by metered dose inhaler and jet nebulizer into neonatal ventilator circuit. Pediatr Pulmonol 1992; 13:172–175.
220. Cameron D, Arnot R, Clay M, Silverman M. Aerosol delivery in neonatal ventilator circuits: a rabbit lung model. Pediatr Pulmonol 1991; 10:208–212.
221. Flavin M, MacDonald M, Dolovich M, Coates G, O'Brodovich H. Aerosol delivery to the rabbit lung with infant ventilator. Pediatr Pulmonol 1986; 2:35–39.
222. O'Callaghan C, Hardy J, Stammers J, Stephenson TJ, Hull D. Evaluation of techniques for delivery of steroids to lungs of neonates using a rabbit model. Arch Dis Child 1992; 67:20–24.
223. Warwick R, Williams PL. Gray's Anatomy. Philadelphia: WB Saunders, 1973.
224. Brown JS, Gerrity TR, Bennett WD, Kim CS, House DE. Dispersion of aerosol boluses in the human lung: dependence on lung volume, bolus volume, and gender. J Appl Physiol 1995; 79:1787–1795.
225. Pritchard JN, Jefferies SJ, Black A. Sex differences in the regional deposition of inhaled particles in the 2.5–7.5 μm size range. J Aerosol Sci 1986; 17:385–389.
226. Bennett WD, Messina MS, Smaldone G. Effect of exercise on deposition and subsequent retention of inhaled particles. J Appl Physiol 1985; 59:1046–1054.
227. Morgan WKC, Ahmad D, Chamberlain JM, Clague HW, Pearson MG, Vinitski S. The effect of exercise on the deposition of an inhaled aerosol. Respir Physiol 1984; 56:327–338.
228. Schulz H, Schulz A, Eder G, Heyder J. Influence of gas composition on convective and diffusive intrapulmonary gas transport. Exp Lung Res 1995; 21:853–876.
229. Svartengren M, Anderson K, Philipson K, Camner P. Human lung deposition of particles suspended in air or in helium/oxygen mixture. Exp Lung Res 1989; 15: 575–585.
230. Anderson M, Svartengren M, Philipson K, Camner P. Deposition in man of particles inhaled in air or helium–oxygen at different flow rates. J Aerosol Med 1990; 3: 209–216.
231. Anderson M, Svartengren M, Bylin G, Philipson K, Camner P. Deposition in asthmatics of particles inhaled in air or helium–oxygen. Am Rev Respir Dis 1993; 147: 524–528.

232. Schulz H, Schulz A, Heilmann P, Heyder J. Can drug delivery to the lungs be influenced by breathing different gas compositions? J Aerosol Med 1993; 6:42s.
233. Garland LH, Beier RL, Coulson W, Heald JH, Stein RL. The apparent sites of origin of carcinomas of the lung. Radiology 1962; 78:1–11.
234. Ferron GA, Brand P, Schulz A, Tippe A, Heyder J. Improvements in deposition modeling. J Aerosol Med 1993; 6(suppl):24.